



Evaluation of atmospheric aerosols in the metropolitan area of São Paulo simulated by the regional EURAD-IM model on high-resolution

Ediclê De Souza Fernandes Duarte^a, Philipp Franke^{b,c}, Anne Caroline Lange^{b,c}, Elmar Friese^{b,c}, Fábio Juliano da Silva Lopes^{d,e}, Jonatan João da Silva^{e,f}, Jean Souza dos Reis^a, Eduardo Landulfo^e, Cláudio Moises Santos e Silva^g, Hendrik Elbern^b, Judith Johanna Hoelzemann^{g,*}

^a Graduate Program in Climate Sciences, Federal University of Rio Grande do Norte, Natal/RN, Brazil

^b Rhenish Institute for Environmental Research at the University of Cologne, Köln, Germany

^c Institute of Energy and Climate Research: Troposphere (IEK-8), Forschungszentrum Jülich GmbH, Jülich, Germany

^d Environmental Science Department, Institute of Environmental, Chemical and Pharmaceutical Science, Federal University of São Paulo, Rua São Nicolau, 210, Centro, Diadema, São Paulo, 09913-030, Brazil

^e Centre for Laser and Applications, Nuclear and Energy Research Institute, São Paulo, Brazil

^f Center for Exact Sciences and Technologies, Federal University of Western Bahia, Brazil

^g Department of Atmospheric and Climate Sciences, Federal University of Rio Grande do Norte, Natal/RN, Brazil

ARTICLE INFO

Keywords:

Mesoscale modeling
Regional transport of aerosols
Model evaluation
Air pollution
Brazil
Urban areas

ABSTRACT

We present a high-resolution air quality study over São Paulo, Brazil with the EUROpean Air Pollution Dispersion - Inverse Model (EURAD-IM) used for the first time over South America simulating detailed features of aerosols. Modeled data are evaluated with observational surface data and a Lidar. Two case studies in 2016 with distinct meteorological conditions and pollution plume features show transport (i) from central South America, associated to biomass burning activities, (ii) from the rural part of the state of São Paulo, (iii) between the metropolitan areas of Rio de Janeiro and São Paulo (MASP) either through the Paraíba Valley or via the ocean, connecting Brazil's two largest cities, (iv) from the port-city Santos to MASP and also from MASP to the city Campinas, and vice versa. A Pearson coefficient of 0.7 was found for PM₁₀ at MASP CENTER and EURAD-IM simulations vary within the observational standard deviation, with a Mean Percentual Error (MPE) of 10%. The model's vertical distributions of aerosol layers agree with the Lidar profiles that show either characteristics of long-range transported biomass burning plumes, or of local pollution. The distinct transport patterns that agree with satellite Aerosol Optical Depth and fire spot images as well as with the ground-based observations within the standard deviations, allows us exploring patterns of air pollution in a detailed manner and to understand the complex interactions between local to long-range transport sources.

1. Introduction

Global air pollution emissions have strongly increased due to transportation, energy production and industrial activities, mostly concentrated in densely populated areas. Such conditions give rise to numerous public health problems such as cardio-respiratory diseases and agents of premature deaths (Saldiva et al., 1994; Faiz et al., 1996; Lanki et al., 2006; Gurjar et al., 2008; Asmi et al., 2009). Environmental impacts are particularly severe in cities of about 10 million or more inhabitants - also

known as megacities. According to United Nations (2018), in 2018, 1.7 billion people, which corresponds to 23% of the world's population, lived in a city with at least 1 million inhabitants, while this number is projected to accrue to 28% by 2030. These cities range from urban areas with relatively clean air in industrialized nations to highly polluted cities in the developing countries (Molina and Molina, 2002, 2004; Molina et al., 2007; Gulia et al., 2015). Thus, megacities tend to be global risk areas due to a dense concentration of people and extreme dynamics. Their inhabitants are vulnerable to air pollution inducing

Peer review under responsibility of Turkish National Committee for Air Pollution Research and Control.

* Corresponding author.

E-mail address: judith.hoelzemann@ccet.ufrr.br (J.J. Hoelzemann).

<https://doi.org/10.1016/j.apr.2020.12.006>

Received 27 July 2020; Received in revised form 7 December 2020; Accepted 9 December 2020

Available online 23 December 2020

1309-1042/© 2020 Turkish National Committee for Air Pollution Research and Control. Production and hosting by Elsevier B.V. All rights reserved.

adverse health impacts (Gurjar et al., 2008). Such risks need to be estimated to support national and international efforts to improve the sustainability of megacity life worldwide.

Atmospheric models with explicit treatment of the physical and chemical processes have become powerful means to the studies of the urban air pollution impacts. A plethora of modeling studies is available focusing on different aspects of the pollution impact, such as pollution episodes (Jiang et al., 2017; Aleksankina et al., 2019), regional and long-distance transport (Tie et al., 2007; Lin et al., 2010; Andrade et al., 2015; Rafee et al., 2017; Albuquerque et al., 2018), secondary formation of gases and particles (Jiang et al., 2012; Lowe et al., 2015; Wang et al., 2005; Wang et al., 2016; Vara-Vela et al., 2018), and the effects of land use and land cover changes (Capucim et al., 2015; Rafee et al., 2015).

In general, Chemistry Transport Models (CTMs) are tools that simulate the formation, transport, chemical transformation, and deposition of particles and gas-phase species. The level of sophistication depends on the degree of complexity of the model by simulating the weather and air quality of a region, it is possible to assess the current level of pollution (Alonso et al., 2010; Vara-Vela et al., 2016, 2018; Albuquerque et al., 2018; Pedruzzi et al., 2019), track trends (Carvalho et al., 2015; Andrade et al., 2015; Zhang et al., 2018), define responsibilities for air pollution levels (Ring et al., 2018; Song et al., 2019), assess the potential impact of future emission sources (Collet et al., 2018; Campbell et al., 2018), study emission reduction scenarios (Alonso et al., 2010; Andrade et al., 2012; Wang et al., 2016; Albuquerque et al., 2019; Yu et al., 2019; Andreão et al., 2020; Pinto et al., 2020) and estimate the health impacts (Boldo et al., 2014; Ding et al., 2016; Andreão et al., 2018, 2020; Li et al., 2019). Applications of regional air quality models across several parts of the world include for example WRF-Chem (Zhang, 2008; Andrade et al., 2015; Rafee et al., 2017; Bahreini et al., 2018), WRF-SMOKE-CMAQ (Albuquerque et al., 2018), BRAMS (Longo et al., 2010; Moreira et al., 2013), POLAIR 3D (Wang et al., 2015); EURAD-IM (Ebel et al., 1997; Elbern et al., 2007, 2010).

In Brazil, many studies have been made by using the Brazilian Regional Atmospheric Modeling System (BRAMS) applied with the purpose of forecasting not only the atmospheric behavior but also air quality (Pielke et al., 1992; Masson, 2000; Rozoff et al., 2003; Cotton et al., 2003; Freitas et al., 2005, 2007a, 2007b, 2007c, 2009, 2017; Longo et al., 2010). Another model that is widely used in Brazil is the Weather Research and Forecast with Chemistry (WRF-Chem) model (Grell et al., 2005). The WRF-Chem model was employed for air quality forecasting in south-eastern Brazil (Andrade et al., 2015), studying how vehicular emissions can affect fine particle formation (Vara-Vela et al., 2016), and quantifying daily and annual PM concentrations in 102 cities (Andreão et al., 2020). These studies showed satisfactory representation of meteorological variables but an overestimation of PM concentrations for some environmental company monitoring stations of São Paulo (CETESB), mainly in MASP. Albuquerque et al. (2018) used the Weather Research and Forecasting-Sparse Matrix Operator Kernel Emissions Models-3 Community Multiscale Air Quality Modeling System (WRF-SMOKE-CMAQ) to represent meteorological and air quality conditions over São Paulo, Brazil, and to evaluate the performance of the model (Albuquerque et al., 2018; Pedruzzi et al., 2019).

Accurate modeling of air pollution must consider atmospheric aerosol processes. The effects of aerosols on meteorological processes and air quality depend largely on their size distribution, chemical composition, mixing state, and morphology (Seinfeld and Pandis, 2016). This is particularly valid for smoke particles in the atmosphere over South America that are annually released from vegetation fires and represent a major aerosol source during the burning season (Hoelzemann et al., 2009). In the vicinity of megacities, urban industrial emissions may be predominant, but on a continental scale sources are mainly composed of carbonaceous aerosol emissions and trace gas emissions from deforestation and savanna maintenance fires. Hundreds to thousands of vegetation fires, primarily in *Cerrado* and Amazon forest

ecosystems, emit vast amounts of aerosol particles into the atmosphere during the burning season and the aerosol effects by fires may go far beyond the local scale and significantly affect the hydrological cycle on a regional scale (Setzer and Pereira, 1991; Artaxo et al., 1998, 2001; Artaxo et al., 2005; Freitas et al., 2005; Freitas et al., 2007c; Hoelzemann et al., 2009). If meteorological conditions are favorable, smoke plumes can be injected into altitudes above the planetary boundary layer (Andreae and Merlet, 2001; Freitas et al., 2007c). Emissions generated from biomass burning contribute extensively to the global budget of several atmospheric constituents such as aerosols, carbon dioxide (CO₂), carbon monoxide (CO), nitrogen oxides (NO_x) and methane (CH₄), amongst others. Hence, fire emissions need to be modeled by global systems that monitor and forecast atmospheric composition, such as the European Copernicus Atmosphere Monitoring Services (CAMS) (Kaiser et al., 2012) and the included in the emission inventories that deliver emission fluxes to the CTM's.

According to Crippa et al. (2018), global emission inventories coupled with CTMs are useful tools to tackle these regional and global aspects, complementing air pollution measurements that provide information on local and regional air quality impacts. Emission inventories tabulate emission rates from individual sources and source categories for the pollutants of interest (Molina and Molina, 2002). Several global emissions inventories have been developed in recent years such as (Monitoring Atmospheric Composition and Climate (MACCity) by Granier et al. (2011), the Hemispheric Transport of Air Pollution Inventory (HTAP v2.2) by Janssens-Maenhout et al. (2015), the Community Emission Data System (CEDS) by Hoesly et al. (2017), the inventory based on Greenhouse Gas and Air Pollution Interactions and Synergies (GAINS), ECLIPSE V5a global emission fields by Klimont et al. (2017) for particulate matter, and the Emissions Database for Global Atmospheric Research (EDGAR) for air pollutants and greenhouse gases calculated in a consistent and transparent way (Crippa et al., 2018).

In the environment of urban areas, the vehicular emissions are becoming increasingly important (Andrade et al., 2017; Ibarra-Espinosa et al., 2018) and measurements have shown that compounds emitted from vehicular exhausts can be highly reactive in the atmosphere, contributing to critical episodes of photo-chemical smog (Nogueira et al., 2015). Although emission inventories are an essential tool for managing and regulating pollution, large uncertainties in emission rates, temporal cycles, spatial distribution, and source identification often confound the development of cost-effective control strategies (Molina and Molina, 2002). In the urban centers of Brazil, the rapid economic growth triggered the increase of the vehicle fleet and therefore increased air pollution (Faiz et al., 1996; Miranda et al., 2012; Andrade et al., 2017; Ibarra-Espinosa et al., 2018). Studies about air quality and its effect on climate and human health for the MASP have been conducted since the 1970s. According to Andrade et al. (2015), in 1960, there was a decrease of air quality with high concentrations of pollutants emitted by industrial activities in the state of São Paulo without any control strategies on the emissions of air pollutants.

The MASP is the largest metropolis in South America, with a population of more than 21 million inhabitants. MASP includes 39 cities covering a surface area of approximately 8000 km² (IBGE, 2020). The climate in the MASP is characterized by temperate oceanic climate (*Cfb*) with wet (October to April) and dry (May to September) seasons. January and June are the hottest and coldest months of the year, respectively (Miranda et al., 2012). MASP suffers from severe air pollution from particulate matter of 10 µm (PM10) as well as 2.5 µm (PM2.5), Ozone (O₃) and aldehydes (Molina and Molina, 2004). During austral winter, unfavorable conditions for pollutant dispersion have been observed, since shallow inversion layers trap pollutants within the lowest 200–400 m height for several days resulting in elevated pollutant concentrations (CETESB 2009; 2017). In comparison with other urban areas of Brazil, the MASP has the best network of air quality monitoring stations, which provide data with the highest spatial resolution by the

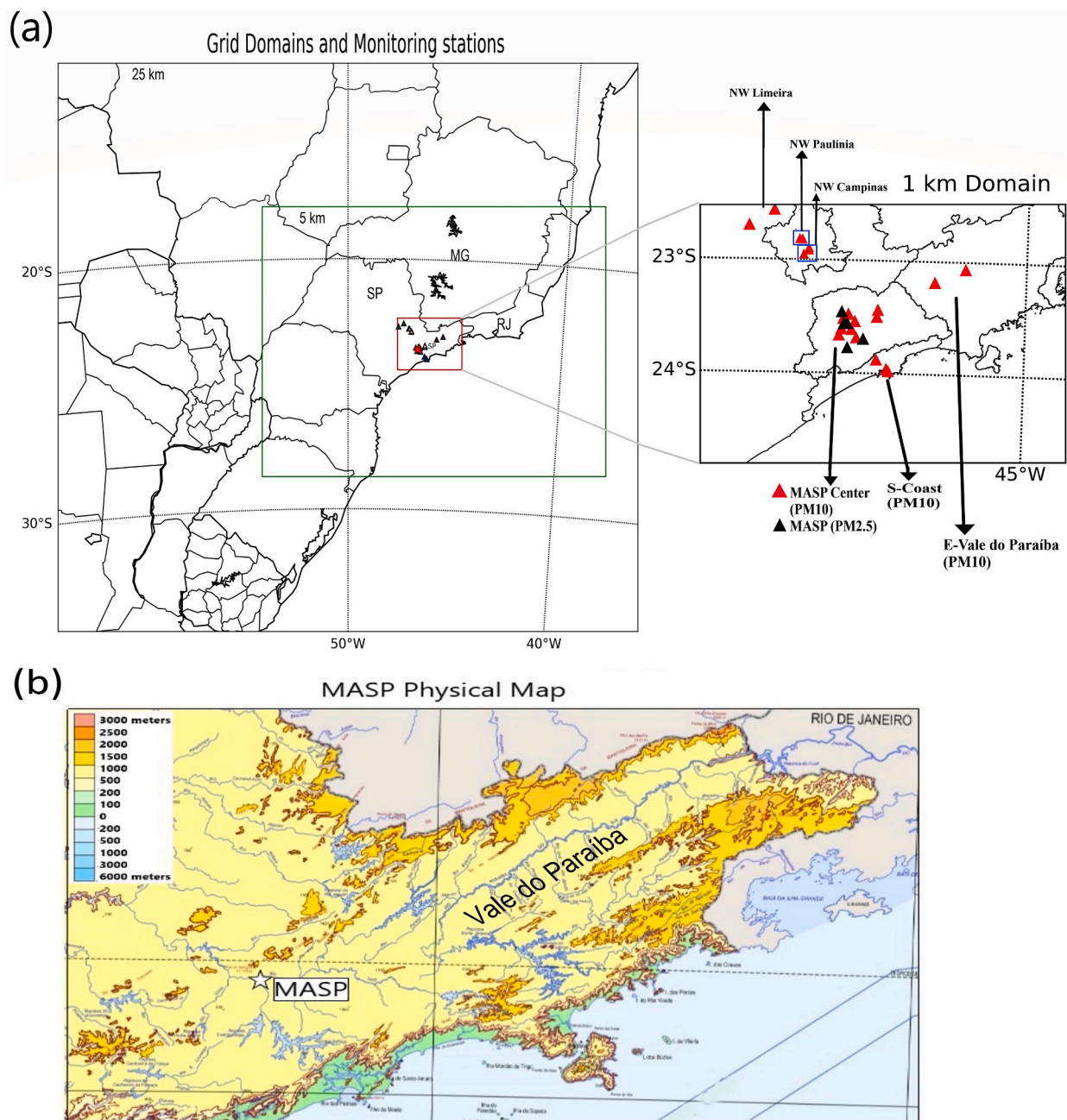


Fig. 1. (a) Allocations of the domains used in the EURAD-IM simulations, the red triangles are PM10 station and black triangles are PM2.5 stations from CETESB locations used in this study, (b) São Paulo physical map. Source: [IBGE \(2020\)](#).

São Paulo State Environmental Sanitation Technology Company (CETESB) ([Andrade et al., 2015](#)).

The objective of this study is to adapt and provide a powerful air quality analysis to investigate the spatial and temporal variability of PM10 and PM2.5 simulated by EURAD-IM during July 10–13, 2016, during the dry season in Southeast Brazil, and October 22–25, 2016, during the transition season from dry winter to wet summer. The EURAD-IM was statistically evaluated and compared to the modeled results on a 1 km² grid resolution with CETESB surface monitoring stations of PM10 and PM2.5, as well as qualitatively with available Lidar profiles. In addition, the model was used to study the regional transport of pollutants to MASP. The period chosen for modeling is related to available observational data in MASP and allows to verify if the EDGAR emission inventory was representative. Meteorological fields were modeled using the Weather Research and Forecasting model (WRF,

[Skamarock et al., 2008](#)), using three nested domains with 25-km, 5-km, and 1-km horizontal grid resolution, which covered the whole southeast of Brazil, São Paulo state, and MASP, respectively.

2. Model and data description

In this section the EURAD-IM air quality model, its respective input data, such as pollutant emissions and meteorological fields are described. Also, the observational data set that has been used to evaluate the model performance over the MASP is presented.

2.1. The meteorological driver model WRF

The WRF Advanced Research (ARW) model, version 3.7, is used to create the meteorological input for EURAD-IM. The WRF model is fully

compressible non-hydrostatic and solves the meteorological equations on a Eulerian grid (Skamarock et al., 2008). The horizontal grid is the ‘Arakawa C’ grid (Arakawa and Lamb, 1977). The meteorological initial and boundary conditions are obtained from United State National Center for Environmental Prediction (NCEP)/National Center for Atmospheric Research (NCAR) Global Forecast System (GFS) at 0.25° resolution, including Newtonian nudging every 6 h (<https://rda.ucar.edu/datasets/ds083.2/>).

In this work, three off-line model domains were used as can be seen in Fig. 1a, the coarse model grid encompasses the major south eastern region of Brazil around São Paulo with 25 km horizontal resolution (domain01). The 5 km resolution domain (domain02) covers the state of São Paulo (SP) while the 1 km resolution domain (domain03) is centered on the MASP at 23.55° S and 46.63° E. The domain01 has 110 × 101 grid points covering an area of 2750 × 2525 km², domain02 has 326 × 241 grid points covering an area of 1630 × 1205 km², and domain03 has 351 × 251 grid points covering an area of 351 × 251 km², three domains with a vertical resolution of 35 layers up to 100 hPa. Fig. 1b shows the topography of São Paulo characterized by flat land, hills, mountains, plateaus and depressions. An important hub connecting São Paulo, Minas Gerais (MG) and Rio de Janeiro (RJ) is the *Vale do Paraíba* (or Paraíba Valley). It is an important passage for commodities, industries and services in the depression between *Serra da Mantiqueira* and *Serra do Mar*.

The main physics parameterizations were chosen based on previous studies such as Andrade et al. (2015), Vara-Vela et al. (2018), Albuquerque et al. (2018; 2019), and Andreão et al. (2020; 2020b) who focus on the region over South America/São Paulo performing air quality simulations. In our simulations the model physics include the Grell 3D ensemble scheme for convection (Grell and Freitas, 2014), the YSU scheme (Hong et al., 2006) for the boundary layer parameterization, WRF Single-Moment 3-class Scheme for the parameterization of cloud microphysics (Hong et al., 2004), the Noah scheme (Tewari et al., 2004) for land surface processes, the RRTM scheme (Mlawer et al., 1997) for longwave radiation and the Dudhia scheme (Dudhia 1989) for shortwave radiation. The meteorological initial and boundary conditions are obtained from GFS meteorological data with 0.25° × 0.25° resolution.

2.2. The EURAD-IM air quality model

The EURAD-IM has been developed to run simulations of meteorological processes, atmospheric chemistry, aerosol dynamics and transport on a regional scale. It is a mesoscale chemistry transport model (Elbern et al., 2007) using WRF as offline meteorological driver. It is used for simulations focusing on emissions and their influence on air quality (Memmesheimer et al., 2000, 2004) as well as for operational forecast down to local scale using the nesting technique. Also, EURAD-IM can be used for episodic scenario forecasts focusing on special aspects of air quality simulations (Ebel et al., 1997; Huijnen et al., 2010; Monteiro et al., 2013; Marécal et al., 2015; Gama et al., 2019) and their analyses using chemical data assimilation and inverse modeling techniques (Elbern and Schmidt, 2002; Elbern et al., 2000, 2007, 2010). The main relevant parts of the forward model are the EURAD Emission Model EEM (Memmesheimer et al., 1991, with later developments), and the kinetic preprocessor, which solves the equations for gas phase chemistry (KPP) (Damian-Jordache, 1996).

To propagate a set of chemical constituents forward in time EURAD-IM solves a system of partial differential equations (Elbern et al., 2007)

$$\frac{\partial c_i}{\partial t} = -\nabla \cdot (\mathbf{v}' c_i) + \nabla \cdot (\rho K \nabla \frac{c_i}{\rho}) + A_i + E_i - S_i, \quad (1)$$

where c_i , $i = 1, \dots, n$ is the mean mass mixing ratios of the n chemical species, \mathbf{v}' is the mean wind velocities, K is the eddy diffusivity tensor, ρ is the air density, A_i is the chemical generation term for species i , and E_i

and S_i describe emission and removal fluxes, respectively.

The Eulerian chemistry transport model applies an operator splitting technique (McRae et al., 1982), where each process in (1) is treated independently in a sequence. In that way different numerical methods, which are specific for the physical character of the processes, can be used efficiently. EURAD-IM uses a symmetric splitting of the dynamic procedures, encompassing the chemistry solver module C (see Hass, 1991),

$$c_i^{t+\Delta t} = T_h T_v D_v C D_v T_v T_h c_i^t, \quad (2)$$

where T_h , T_v and D_v denote transport and diffusion operators, respectively, in horizontal (h) and vertical (v) directions. The emission term is included in C , the spatial discretization indices are omitted here. Concentration changes due to cloud effects are calculated at hourly intervals. During the cloud lifetime of 1-h aqueous phase chemistry and scavenging effects are integrated with time steps limited by these specific processes.

The CTM uses the aerosol module Modal Aerosol Dynamics model (MADE) (Ackermann, 1997; Ackermann et al., 1998), which is derived from the Regional Particulate Model (RPM) (Binkowski and Shankar, 1995). The aerosol size distribution is represented by three log-normal modes, i. e. - Aitken ($d < 0.1 \mu\text{m}$), accumulation ($0.1 < d < 1 \mu\text{m}$), and coarse ($d > 1 \mu\text{m}$) mode with standard deviations of $\sigma_{\text{Aitken}} = 1.7$, $\sigma_{\text{Accumulation}} = 2.0$, and $\sigma_{\text{coarse}} = 2.2$, respectively. The chemical species treated in the finer aerosol modes are secondary inorganic components (sulfate, nitrate, and ammonium), secondary organic components of biogenic or anthropogenic origin, primary organic carbon, elemental carbon, and other unspecified material of anthropogenic origin. The coarse mode species include sea salt, wind-blown dust, and other unspecified material of anthropogenic origin. The anthropogenic component of the coarse particles is most often attributed to industrial processes (Ackermann, 1997; Ackermann et al., 1998). Each aerosol mode is subject to wet and dry deposition. The chemistry mechanism for the gas-phase is the RACM-MIM, developed by Geiger et al. (2003). It is based on the Regional Atmospheric Chemistry Mechanism (RACM) (Stockwell et al., 1997) mechanism combined with the Mainz Isoprene Mechanism (MIM) (Pöschl et al., 2000) and reflects an advanced description of the air chemistry of biogenic ozone precursors. It treats 84 chemical species (as real species and condensed species classes) and contains 23 photolysis reactions and 221 chemical reactions of higher order.

2.3. Emissions

The EURAD Emission Module (EEM) prepares emission data for chemistry-transport-calculations. The EEM acts as an interface between the emission inventories available for certain areas and time periods to be simulated in the CTM. The EEM projects the emission inventory data spatially on to the numerical grid and computes the desired emission rates with a temporal resolution of 1 h. The emissions are transformed from the original grid to any EURAD-IM grid and dis-aggregated to the source of the emission, if available. The variability of emissions due to seasonal, weekly, or daily cycles is incorporated in EEM output using hour-of-day, day-of-week, and monthly emission factors to distribute the total annual emissions temporally as described in Simpson et al. (2012). For a more detailed description see Memmesheimer et al. (1991).

In this study the EDGAR inventory v4.3.2 (Crippa et al., 2018) was used. EDGAR covers gaseous air pollutants of Carbon Monoxide (CO), Nitrogen Oxides (NO_x), Sulfur Dioxide (SO₂), total Non-Methane Volatile Organic Compounds (NMVOC) and ammonia (NH₃). As to the aerosols PM10, PM2.5, and carbonaceous species BC and OC are provided. Its database was built considering the location of power and manufacturing facilities, road networks, transportation routes, human and animal population density, and agricultural land use, which vary over the years. Country emissions are then compiled considering the

Table 1
SNAP source sectors (Eurostat, 2004).

SNAP 1	Combustion in energy and transformation industries
SNAP 2	Residential and non-industrial combustion
SNAP 3	Combustion in the manufacturing industry
SNAP 4	Production processes
SNAP 5	Extraction and distribution of fossil fuels
SNAP 6	Solvent and other product use
SNAP 7	Road transport
SNAP 8	Other mobile sources and machinery
SNAP 9	Waste treatment and disposal
SNAP 10	Agriculture

International Energy Agency (IEA) energy statistics. The total national emissions are gridded using population, road, power plants, animals, and crop proxy data. Air quality modeling using EDGAR was performed with focus on primary particles (PM₁₀, PM_{2.5}) for the three domains with 25 km, 5 km and 1 km horizontal resolution. The EURAD-IM uses MADE to calculate initial number concentrations from given mass concentrations and from there calculates the minimum median diameters of the particles. The aerosol chemistry encompasses the formation of secondary aerosols formed by gas-to-particle conversion of inorganic and organic precursors. The formation and partitioning of secondary organic aerosols (SOA) are simulated by the Secondary ORGANIC Aerosol Model (SORGAM) coupled to MADE. In the case of elemental carbon, organic carbon, and other fine particles of anthropogenic origin emissions are compiled from land-use characteristics and emission inventories (in this case, EDGAR) and delivered for each model grid. They are subject to seasonal, weekly, and diurnal variations. Additionally, the EURAD-IM calculates mineral dust emissions and sea salt emissions out of the turbulent flux using the parameterization of Monahan (1988) is used, which estimates the flux depending on the particle size.

All emissions are split across a set of emission source sectors defined by the Selected Nomenclature for Air Pollutants (SNAP) as described in Table 1. Here, SNAP 10 is assigned to agricultural emissions, describing all anthropogenic emissions from this sector including on-site burning of residue from main crops harvested for dry grain (such as soy), burning of sugar cane crop residue and on-site burning of residue from crops not mentioned above.

2.4. Chemical initial and boundary conditions

To obtain realistic initial conditions for the EURAD-IM simulations, a model spin-up of three days was performed, starting from Copernicus Atmosphere Monitoring Service (CAMS) fields (Inness et al., 2019) to provide realistic three-dimensional analysis for initial values for the desired episodes. CAMS is the latest global reanalysis dataset of atmospheric composition produced by the European Center for Medium-Range Weather Forecast (ECMWF) consisting of three-dimensional time-consistent atmospheric composition fields, including aerosols and chemical species. CAMS provide global analysis and forecasts of atmospheric composition, alongside European air quality forecasts (Hollingsworth et al., 2008) using the CAMS Integrated Forecasting System (C-IFS) model (Morcrette et al., 2009; Benedetti et al., 2009; Peuch and Engelen, 2012; Flemming et al., 2015).

Boundary values for the nested grids are obtained from their respective mother grids. From available measurements of the transported species latitude-dependent vertical profiles are derived and equally distributed over the whole model domain. For the coarsest grid, chemical boundary conditions of the EURAD-IM model also use CAMS reanalysis, based on global emission datasets that include anthropogenic emissions from the Monitoring Atmospheric Composition and Climate/CityZen (MACCity) inventory (Stein et al., 2014) and biomass burning emissions from the Global Fire Assimilation System (GFAS) data set (Kaiser et al., 2012). Great care has been taken to ensure that the emission datasets used in CAMS were consistent in time and that

consistent anthropogenic, biogenic and biomass burning emissions were used in the aerosol and chemistry modules (Inness et al., 2019).

2.5. Observational data

The EURAD-IM model is validated against observational in-situ data from the operational monitoring network of the São Paulo state environmental agency CETESB and a Lidar which are introduced in the following. Fig. 1a shows the locations of the CETESB stations and the Lidar.

2.5.1. CETESB in situ data

In 2016, CETESB operated 60 fixed automatic stations, out of which 29 stations were located within the MASP, while the others 31 stations are distributed in the inland and at the coast. These stations measure concentrations of PM₁₀, PM_{2.5} as hourly means. The method used by CETESB's automatic monitoring stations to measure the concentration of PM suspended in the atmosphere is absorption by beta radiation. This measurements technique is widely used for operational use as it provides a high accuracy. In this study, 20 sites of PM₁₀ and 5 sites of PM_{2.5} CETESB automatic station were used to evaluate and compare with model results for a 1 km domain, as shown in Fig. 1a. Neighboring stations, which are assumed to be exposed to a similar chemical regime, were grouped into 8 clusters of super-observations (Table S1). Further, the Pearson's correlation coefficient, RMSE and Bias for each cluster were calculated.

2.6. Characterization of the case studies

Two case studies were carried out. The first one during the winter-time (characterized as dry season), for the days of July 10–13, 2016, and the second one during the springtime (transition to wet season), for the days October 22–25, 2016, in southeastern Brazil. During most of the dry season in SP state, frequent subsidence and thermal inversion layers provide unfavorable conditions for the dispersion of pollutants (Albuquerque et al., 2012) and biomass burning emissions are transported from different parts of Brazil and South America (Hoelzemann et al., 2009; Miranda et al., 2017; Vara-Vela et al., 2018) to the south and southeast Brazil. During spring in southeastern Brazil, the rains become more intense and frequent, marking the transition period between the dry season and the rainy season.

According to CETESB (2016), the year 2016 was marked by a neutral situation of oceanic and atmospheric conditions in the Equatorial Pacific region, indicating the end of the global scale phenomenon El Niño-Southern Oscillation (ENSO) that had acted throughout 2015 and lead to atmospheric blockings, both in the Pacific and in the Atlantic Ocean. The latter influenced the rainfall regime, varying between very rainy months and dry and hot months in the State of São Paulo. In contrast to the situation in 2015, July and September 2016 were, in general, more wet than the climatological average (CETESB, 2016). The year 2016 was marked by favorable weather conditions for the dispersion of air pollutants. According to data from CETESB, the period from May to September is generally the most favorable for high pollution episodes as the free dispersion of primary pollutants in the State of São Paulo is hampered by a very stable atmosphere and frequent thermal inversion events. In winter 2016, only 25 days were counted as favorable for pollution episodes which is the lowest in the last ten years (CETESB, 2016).

Significant events of long-range and regional transport of aerosols into the MASP are often observed, especially during the winter period of South America. Two of the 2016 aerosol transport events coincided with local measurements of aerosols properties by the Lidar of MASP and CETESB surface station data. The first event occurred from July 10–13 during the dry season and the second from October 22–25 during the onset of the wet season. Both events show distinct meteorological conditions that contribute in very different ways to increase air pollution

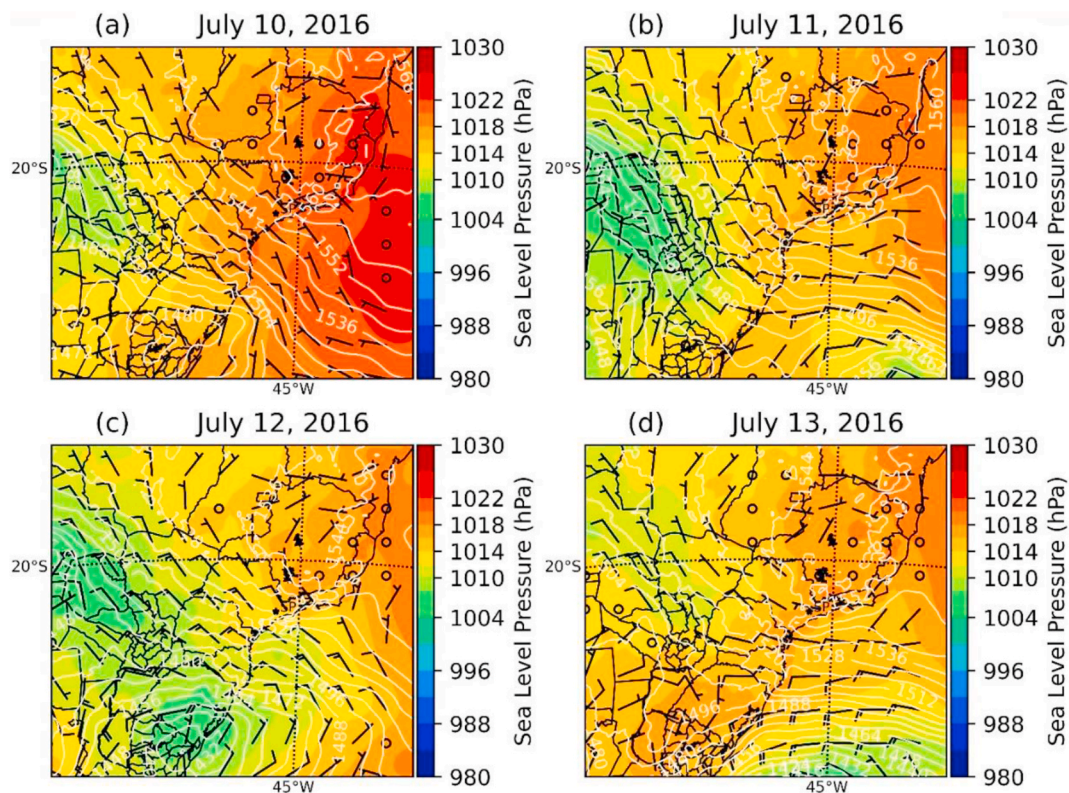


Fig. 2. Sea level pressure (hPa) (color code jet), wind (m/s) at 850 hPa and Geopotential height (m) at 850 hPa represented by the white lines simulated by the WRF for July (a) 10, (b) 11, (c) 12, and (d) 13, 2016, daily average on the 25-km resolution grid.

concentrations in the MASP.

3. Results and discussion

3.1. Case study July 10–13, 2016: dry season in southeast Brazil

The statistics indices obtained from the comparison between hourly observed and modeled meteorological parameters are presented in section S4: “Meteorological validation” in the supplementary material. Fig. 2 shows the meteorological situation on the 25 km model domain for July 10–13. It is important to note that the wind speed and direction at 850 hPa (about 1400 m a.g.l.) indicate air masses coming from the Amazonian basin associated with the South American Low-Level Jet (SALLJ). The SALLJ is an important driver of long-range transport of pollutants to South and Southeast Brazil (Marengo et al., 2004; Freitas et al., 2005, 2007a, 2007b, 2007c; Vera et al., 2016; Martins et al., 2018). Most of the SALLJ passed over and through São Paulo towards the Southern Atlantic Ocean during this first case study.

Since July 10, São Paulo state had been under the influence of a closed high-pressure system of approximately 1022 hPa (Fig. 2a). While a previous low-pressure system was moving east from the southern Atlantic to the south of Brazil, a second one was arriving from Bolivia and Paraguay with a central pressure of about 998 hPa (Fig. 2b). This synoptic condition was accompanied by deep convection systems in São Paulo state. The associated high-pressure system was not so strong over the continent during the following days over the region (Fig. 2c and d). A second extratropical cyclone coming from the Pacific Ocean passed the Andes Mountains cordillera at the latitude of 22° S and built a new cold front over the Atlantic Ocean that extended its influence over the continent at latitudes of the southern region of Brazil on the days of July 12–14. The low-pressure system moved quickly to the east and the SALLJ lost its configuration in the following hours. The wind magnitude over MASP was about 10 m/s and wind direction represented by wind

barbs at 850 hPa were pointed to the Southeast reaching the MASP, which means that the SALLJ affected MASP in that case.

Fig. 3a and Fig. 3b present the Aerosol Optical Depth (AOD) from Terra and Aqua (MYD04_L2) satellites at 3 km resolution for day time overpasses (Levy et al., 2013), Suomi National Polar-Orbiting Partnership (S-NPP) the merged dark target/deep blue AOD layer (Hsu et al., 2013, 2019; Sayer et al., 2017) as well as the MODIS fire hotspots products from the Terra (MOD14) and Aqua (MYD14) satellites for July 11 and 12, 2016. Fig. 3a and b show the tropospheric AOD column varying between 0 and 3 over São Paulo state, reaching a value of 5 over the Southeast Atlantic Ocean and Central Brazil. High values of AOD in central Brazil are in the same location as the high number of fire counts, which indicates relation to aerosol load from biomass burning origin.

On July 12, the fire hotspots were most abundant in Central Brazil, a region between the states of Goiás (GO), Tocantins (TO) and the Federal District (DF), with predominant *Cerrado* biome. *Cerrado* is the second most extensive vegetation formation in South American, with an area of more than 2 million square kilometers (IBGE, 2016). Its area represents one fourth of Brazil’s entire land surface. According to data from INPE for 2016, the *Cerrado* had approximately 151.142 km² of its area burnt, whereas a total area of 280.970 km² burnt in the whole country (Libonati et al., 2015; Rodrigues et al., 2019). For the month of July, the total area burned at *Cerrado* was 21.514 km², while in the Amazon, it was 4.514 km² (INPE, 2016). This biomass burning activity in Central Brazil has a significant impact on the long-range transport of air pollutants to and across Southeast Brazil.

The state of São Paulo also presented biomass burning activities in its center, northwest of the MASP. The aerosols emitted by these fire activities, reached higher levels of the atmosphere (up to 500 hPa) and are transported to regions more distant from their point of origin (Hoelzemann et al., 2009; Miranda et al., 2017; Vara-Vela et al., 2018). The state of São Paulo engages in intense sugarcane production, which is also associated with an annual burning process shortly before or during

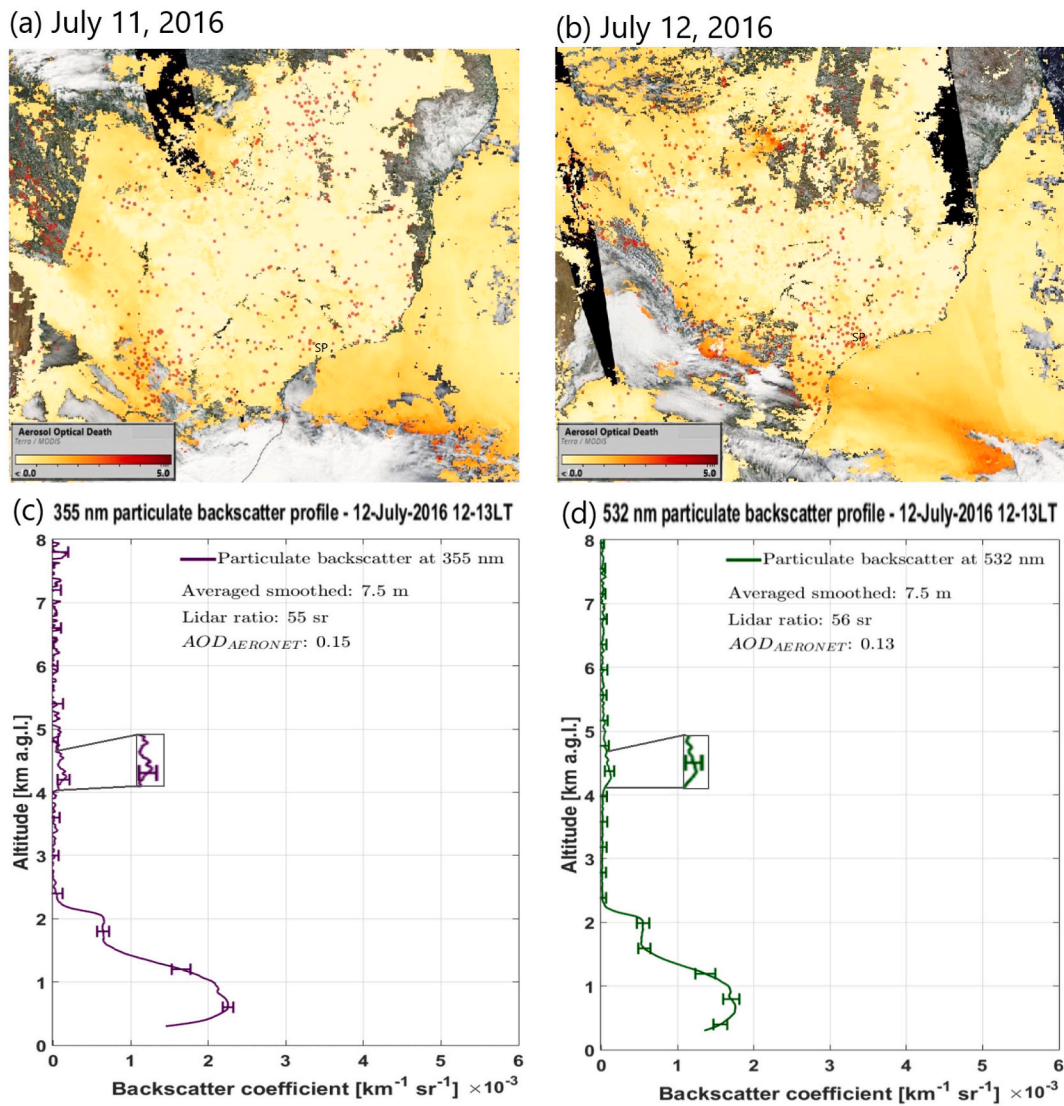


Fig. 3. (a) and (b) Compiled satellite AOD columns from Terra (MOD04_L2) and Aqua (MYD04_L2), Suomi NPP/VIIRS Deep Blue Aerosol Optical Depth layer, MODIS AOD (MOD04_3 K) and Aqua (MYD04_3 K) and associated MODIS fire hotspot products (red dots) for July 11 and 12, respectively (Source: NASA, 2020); The Backscatter profiles for July 12, 2016, between 1200 and 1300 h LT from the IPEN Lidar in the MASP at: (c) 355 and (d) 532 nm.

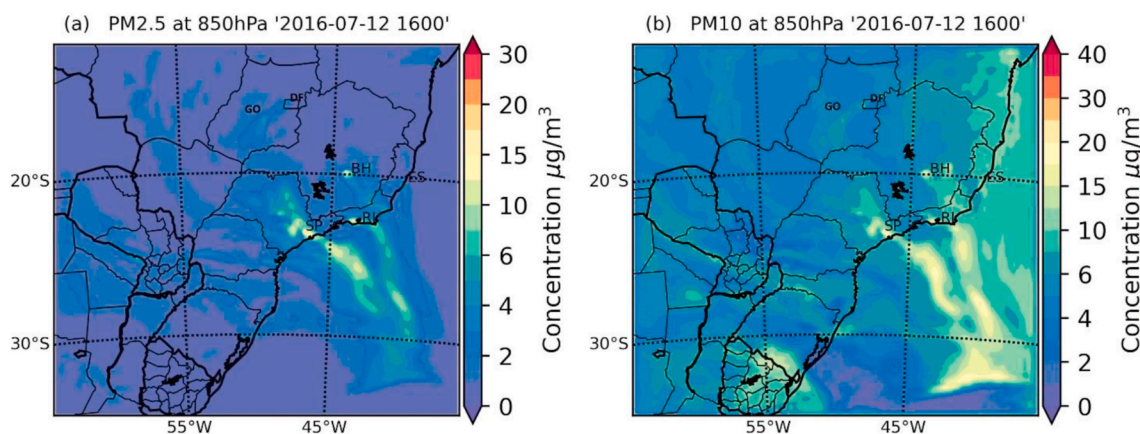


Fig. 4. Aerosols simulations of EURAD-IM on the 25-km domain (a) PM_{2.5} and (b) PM₁₀ concentrations at 850 hPa on July 12, 2016 at 1600 LT.

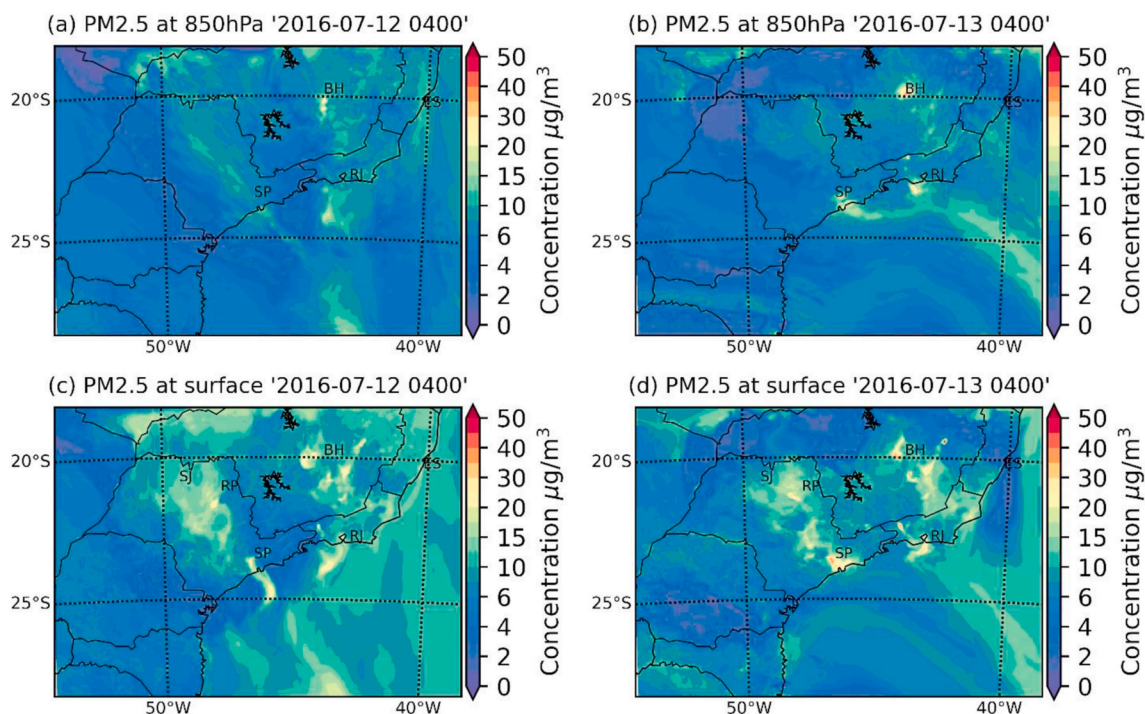


Fig. 5. PM2.5 concentration simulated by EURAD-IM with 5-km horizontal resolution at 0400 LT at 850 hPa on July 12 (a), and July 13(b) (top panels), and at surface on July 12 (c), and July 13 (d) (bottom panels).

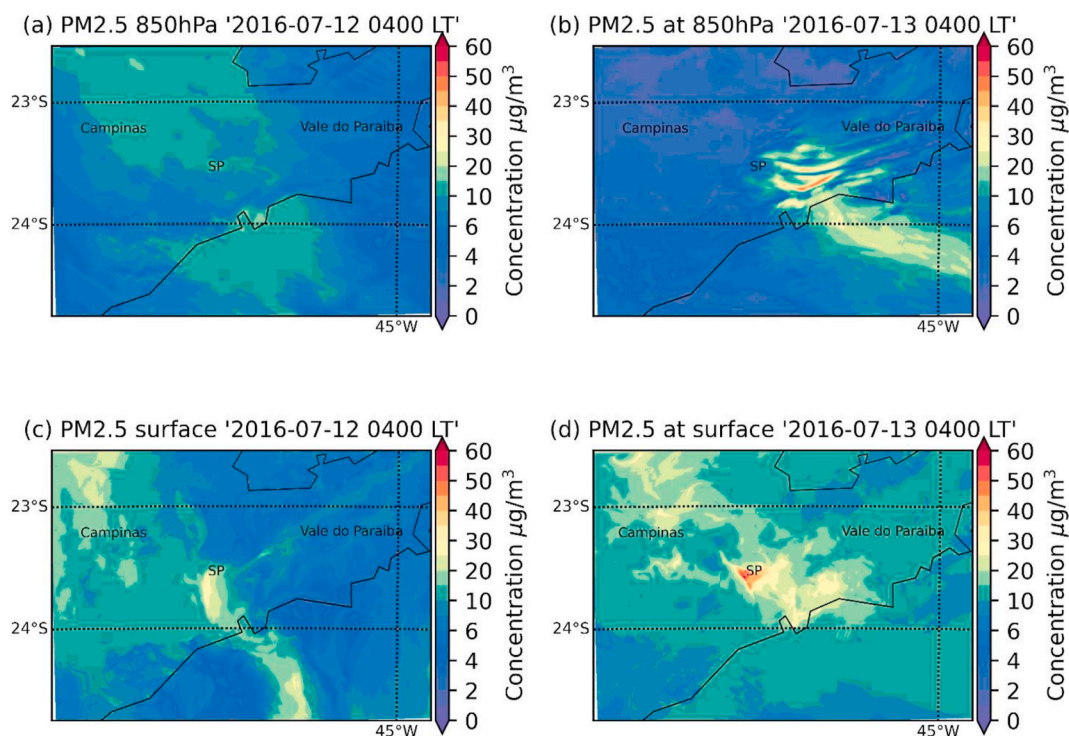


Fig. 6. PM2.5 concentrations simulated by EURAD-IM on the 1-km resolution grid at 850 hPa, 0400 LT for (a) PM2.5 on July 12; (b) PM2.5 on July 13 and at surface for (c) PM2.5 on July 12; (d) PM2.5 on July 13, 2016.

harvesting (Allen et al., 2009; Vasconcellos et al., 2010; Souza et al., 2014; Andrade et al., 2017). Although legislation has been prohibiting this practice along with general agricultural waste burning in the more recent years, it is still very common within the state of São Paulo throughout the year (e.g. Kumar et al., 2016).

Through the analysis of the Lidar vertical profiles it is possible to

detect the different aerosols layers and their heights (see topic S1: “Methodology of Lidar profiles of aerosol properties for São Paulo”). Merging this information with an air quality model, it is possible to study the origin and the transport of aerosols in the atmosphere. Fig. 3c and d shows the mean vertical profiles of aerosol backscattering coefficients for 355 nm and 532 nm respectively for July 12, retrieved by

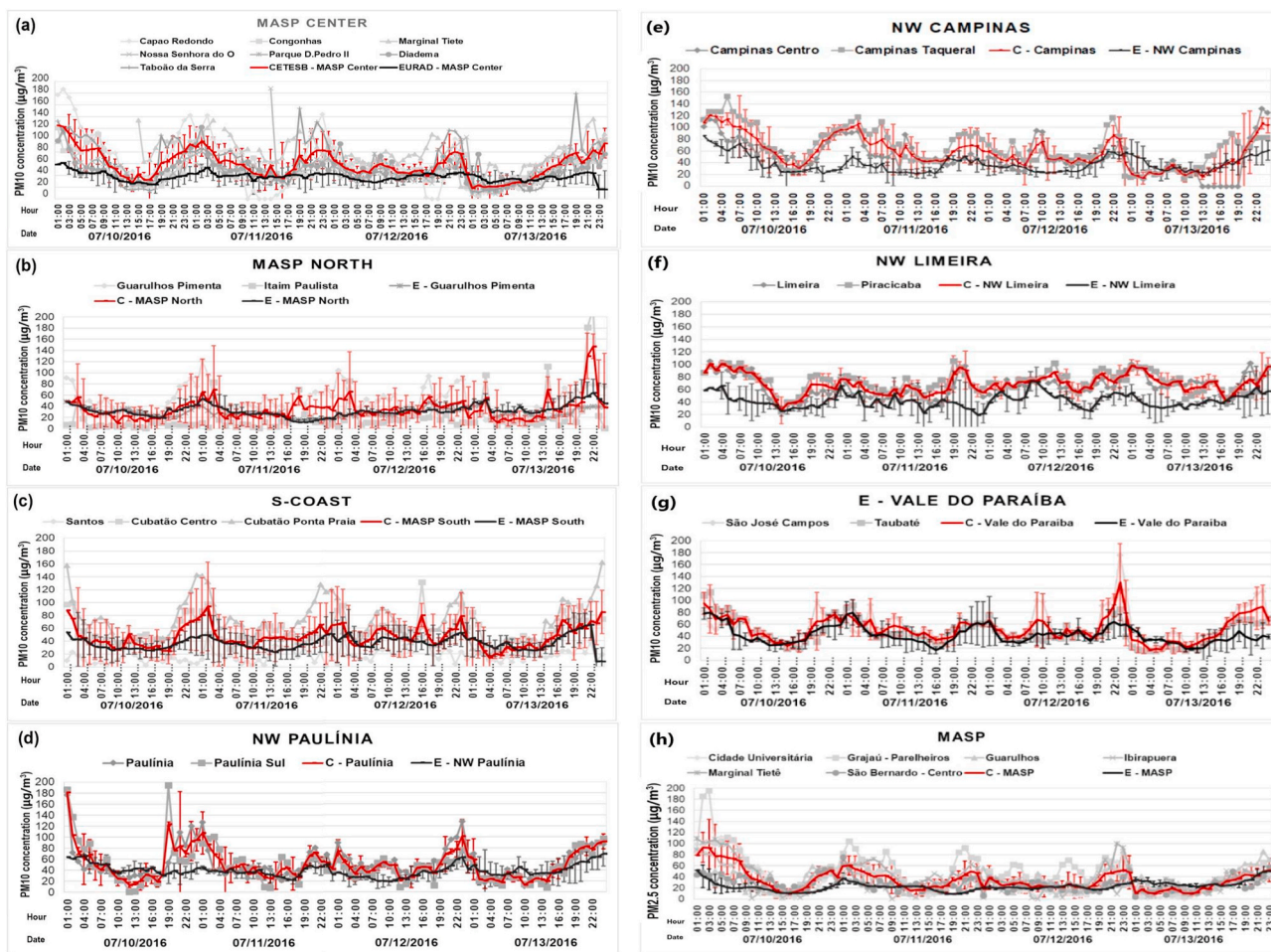


Fig. 7. PM10 concentrations for July 10 to 13, 2016 as measured by CETESB stations and modeled by EURAD-IM. For each CETESB super-observation (red) the original data at the observation sites (grey) and EURAD-IM super-observation (black) are given. Further, Table S1 defines the cluster grouping.

Table 2

Model quality indicators calculated with hourly concentration observed/ modeled from July 10–13 in 26 background sites (20 PM10 and 5 PM2.5) grouping in 8 Clusters according to Table S1.

Cluster	r	RMSE	Bias
MASP Center (PM10)	0.72	30.85	−37.70
MASP North (PM10)	0.50	17.95	−8.80
NW Paulínia (PM10)	0.55	26.12	−22.10
NW Campinas (PM10)	0.61	29.73	−35.50
NW Limeira (PM10)	0.50	30.04	−38.60
S-Coast (PM10)	0.68	16.75	−20.70
E-Vale do Paraíba (PM10)	0.67	18.35	−20.30
MASP (PM2.5)	0.38	20.77	−32.20

applying the KFS inversion method to the data obtained from the SPU-Lidar system in the MASP. Both profiles show that most of the aerosol load in the atmosphere is concentrated within the PBL, approximately up to 2100 m (a.g.l.) showing a peak of $0.0017 \text{ km}^{-1} \text{sr}^{-1}$ at approximately 700 m. However, a very thin aerosol layer can clearly be seen above the PBL, between 4000 and 4700 m a.g.l. - which would typically be from a source outside the MASP. Typically, this type of intrusion is often related to biomass-burning aerosol transported from remote locations outside MASP. However, for this case the total column Lidar ratio at 532 nm is 56 sr and can be associated to less absorbing urban particles (Weitkamp, 2005).

EURAD-IM results on the 25-km domain at 850 hPa on July 12, 1600 Local Time (LT) are presented as PM2.5 concentrations in Fig. 4a and

PM10 concentration in Fig. 4b. On this day a plume located at latitude 18° S and longitude 50° W , which is at the border between the states Goiás (GO) and Brasília (DF), travelled about 700 km following the trajectory of the SALLJ and reached SP state. In Fig. 4a elevated PM2.5 concentrations of agricultural waste burning origin can be seen over Sao Paulo state. This plume mixed with the aerosol layer coming from the fires in central Brazil, forming a mixed aerosol layer on the way to the MASP.

Fig. 5a and Fig. 5b depict the PM2.5 concentrations as simulated by the EURAD-IM on the 5-km domain at 850 hPa, on July 12 and 13 at 0400 LT. The time was chosen for both days because they best represent the regional transport at 850 hPa coming from other regions of Brazil, Fig. S1 presents simulation between July 12, 0400 LT to July 13, 1200 LT. Fig. 5a, in line with Fig. 4, indicates that the plume from Goiás and Brasília reaches the state of São Paulo. Fig. 5b shows the mixing of PM2.5 plumes produced by the MASP and the Metropolitan Area of Rio de Janeiro (MARJ) over the ocean. Thus, the SALLJ that passes through SP state not only transports pollution from Central Brazil to São Paulo but also transports pollutants to MARJ via the Atlantic coastal region between the states of São Paulo and Rio de Janeiro. The PM10 EURAD-IM simulations shows a similar behavior as those of PM2.5, which are shown in Fig. S2.

Fig. 5c and d show the PM2.5 concentrations at surface on July 12 and 13, respectively, at 0400 LT. The impact of agricultural waste burning emission in São Paulo state is more evident, reaching values of about $30 \mu\text{g}/\text{m}^3$ at the municipality Ribeirão Preto (RP) and also at São José do Rio Preto (SJ), considered as an industrial and agricultural area

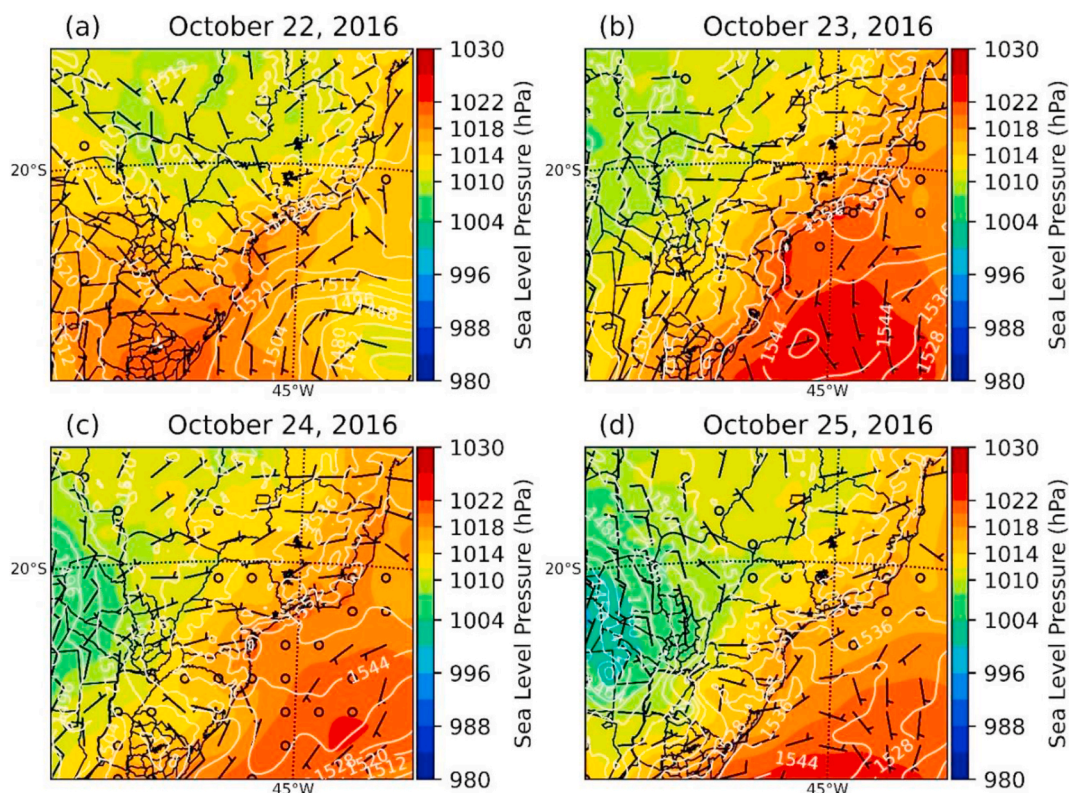


Fig. 8. Sea level pressure (hPa) (color code jet), wind (m/s) and geopotential height (m) at 850 hPa represented by the white lines simulated by WRF for October (a) 22, (b) 23, (c) 24 and (d) 25, 2016, with 25 km horizontal resolution.

in the State of SP according to CETESB (2016). EDGAR emissions showed a predominance of emissions of Agricultural activities (SNAP 10) and Waste treatment and disposal (SNAP 09) in the region (Fig. S5). The EURAD-IM simulations on the 5 km domain show that the resolution significantly affects the concentration of total PM_{2.5}, especially the maximum and minimum values over the MASP, as model values represent an average of each grid cell's volume. Fig. 5 also depicts significant impact of other urban centers such as the metropolitan regions as Rio de Janeiro and Belo Horizonte in the state of Minas Gerais on the PM concentrations. These urban centers yield high concentrations of both coarse and fine aerosols.

Fig. 6 presents the PM_{2.5} concentrations on the 1-km domain at 850 hPa and at surface for July 12 and 13 at 0400 LT, respectively. At this resolution the higher PM concentrations transported by SALLJ can be clearly identified. July 12 at 0400 LT was chosen because it best represents the moment that pollutant plumes are reaching MASP through the SALLJ mix with pollution generated by the MASP during the day. On July 13, at 0400 PM_{2.5} plumes are being lifted over MASP and move to the direction of MARJ (Fig. S1 and Fig. S2 show July 12 at 0400 LT to July 13, 1200 LT for PM_{2.5} and PM₁₀ at 850 hPa). The synoptic conditions for July 12 (Fig. 2c) show that wind direction at 850 hPa was pointing to southeast in the direction of the ocean and the low-pressure system was over the south of Brazil. On July 13 the low-pressure system moved over the ocean (Fig. 2d) changing the wind direction and favoring the displacement of pollutants from SP to RJ. The EURAD-IM results for the period of July 12 showed that the pollution generated by MASP, where industrial and vehicular emission were predominant. These pollutants are added to the pollution that originated from Central Brazil and the interior of SP state, where also intensive agricultural and industrial activities occur. The wind at 850 hPa reaching MASP is coming from the Northwest (Amazon Basin and Central Brazil, see Fig. 2). Downwind of MASP the plumes with elevated PM concentrations turn towards the Northeast or North where they are channeled through

the Paraíba Valley or transported along the coast of São Paulo state to Rio de Janeiro state (Fig. 6b).

We extracted the concentration of total PM₁₀ and PM_{2.5} at 850 hPa upwind the urban area of MASP, and assumed this value as roughly conserved when entering the city area: without significant time for deposition or a major amount of other components than biomass burning in the plume. We set the total PM, with the local city PM emissions added, in ratio to the upwind value. According to the wind speed and direction, we estimated that the contribution of PM₁₀ from the interior of SP was 47% of the total mass of PM₁₀ in the city at 850 hPa for July 12–13, while for PM_{2.5} it was 50%. Of this total PM₁₀ at MASP, 13% contributed to increase the concentration of PM₁₀ in the of Vale do Paraíba advected by the winds and 30% of total PM₁₀ from MASP contributed to the increased PM₁₀ over Santos. For PM_{2.5} the contribution was 21% for Vale do Paraíba and 50% for Santos.

Fig. 7 presents the comparison considering in-situ observations of PM₁₀ and PM_{2.5} surface concentration at 26 CETESB stations and modeled EURAD-IM simulations at the coinciding 26 grid boxes of the 1 km domain. Neighboring stations, which are assumed to be exposed to a similar chemical regime, were grouped into 8 clusters of super-observations, according to Table S1. Further, the Pearson correlation coefficient, RMSE and bias for each cluster were calculated in Table 2.

Table 2 presents statistical indexes for PM₁₀ and PM_{2.5}. At the surface level, the model reproduced the behavior of observed PM₁₀ concentrations but underestimated the observations with a moderate positive Pearson correlation for clusters outside MASP CENTER. In the cluster MASP NORTH, S-Coast and E – VALE DO PARAÍBA - Fig. 7b, c and g, the EURAD-IM were inside the standard deviation of observations presenting a correlation coefficient of 0.50, 0.68 and 0.67, respectively, which is a moderate positive relationship according to Wechsler (1996). The EURAD-IM performs especially well for the cluster MASP CENTER (Fig. 7a) where the observational grid is denser. The Pearson coefficient was 0.72, with a variance of RMSE = 30.85, and underestimated the

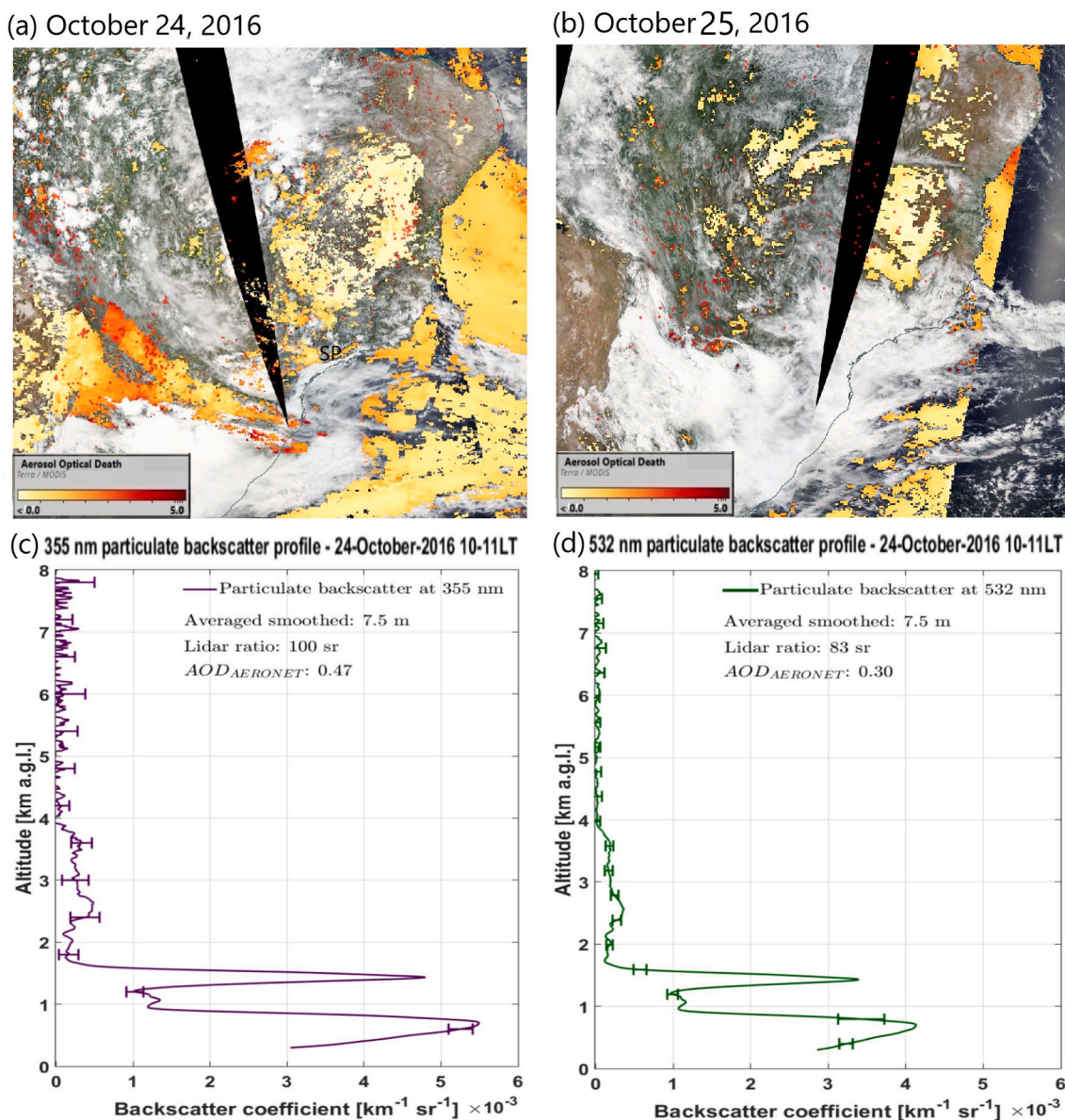


Fig. 9. AOD from Terra (MOD04_L2), Aqua (MYD04_L2), MODIS Fire hotspots and Thermal Anomalies product from Terra (MOD14), Aqua (MYD14) across Brazil and other South American countries (a) on October 24, 2016 and (b) on October 25, 2016 (Source: Nasa, 2020); the Backscatter backscatter profiles on October 24, 2016, between 10:30 and 11:30 LT from the IPEN Lidar in the MASP at: (c) 355 and (d) 532 nm.

observations (bias = -37.70). For PM_{2.5} Pearson's correlation was $r = 0.36$ at MASP with EURAD-IM underestimating the observations by (bias = -32.20) (more information about model performance are in session S5, in the supplementary material). The model better represented the daytime PM₁₀ concentrations, where more CETESB monitoring stations were available.

At S-Coast (see location in Fig. 1) EURAD-IM lies inside the standard deviation of the observations that for this area englobes the CETESB stations of Santos, Santos Ponta da Praia and Cubatão. This area is characterized as an important industrial area of the MASP and road transport is also a large source of pollution, which can dominate pollutant concentrations at ground level, depending on meteorological conditions. Dispersion is restricted by surrounding mountain ranges (Allen et al., 2009). The pollution generated by the port and industrial region of S-Coast is influenced by the sea breeze that transports this pollution at times to MASP through the sea-breeze front toward the center of the city (Freitas et al., 2007a,b). S-Coast pollution can also be transported to regions as MARJ or southward and south-eastward along

the Atlantic coast.

For the other clusters, the correlation varied between 0.5 and 0.7. The model also reflects the morning (0500–0900 h LT) and the evening rush hour (1700–2000h LT) well, during which very high traffic emissions are the rule. Especially at the evening, after 1700 LT, the PM concentration increases for all cluster during July 10–13, due to traffic emission and unfavorable weather condition for pollutants dispersion. For July 11, PM₁₀ reaches a peak at 0100 LT for all clusters (C - MASP CENTER = $94 \mu\text{g}/\text{m}^3$, E - MASP CENTER = $40 \mu\text{g}/\text{m}^3$; C - MASP North = $65 \mu\text{g}/\text{m}^3$, E - MASP North = $40 \mu\text{g}/\text{m}^3$; C NW Paulínia = $108 \mu\text{g}/\text{m}^3$, E - NW Paulínia = $44 \mu\text{g}/\text{m}^3$; C-NW Campinas = $96 \mu\text{g}/\text{m}^3$, E - NW Campinas = $41 \mu\text{g}/\text{m}^3$; C-NW Limeira = $76 \mu\text{g}/\text{m}^3$, E - NW Limeira = $50 \mu\text{g}/\text{m}^3$; C - S-Coast = $80 \mu\text{g}/\text{m}^3$, E - S-Coast = $49 \mu\text{g}/\text{m}^3$; C - Vale do Paraíba = $76 \mu\text{g}/\text{m}^3$, E - Vale do Paraíba = $57 \mu\text{g}/\text{m}^3$) and for PM_{2.5} at MASP as well, C - MASP = $60 \mu\text{g}/\text{m}^3$, E - MASP = $37 \mu\text{g}/\text{m}^3$. Similar peaks of PM₁₀ and PM_{2.5} concentrations occur for the following days in the evening after 1700 LT until later night (Fig. 7). The large number of vehicles circulating in the city at these times match with the low height

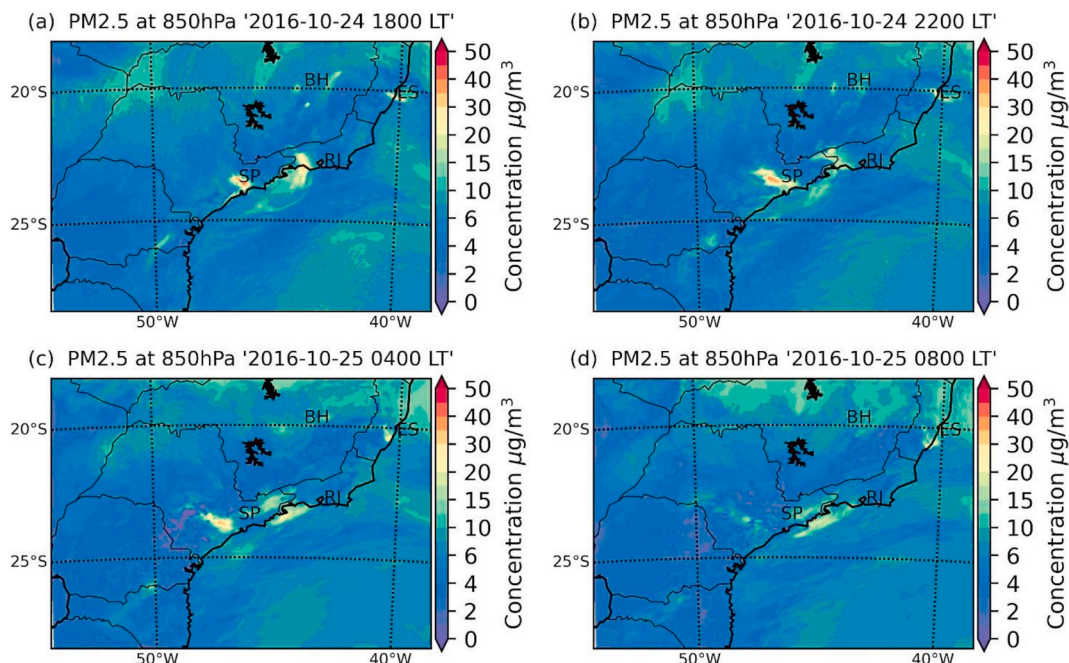


Fig. 10. EURAD-IM simulations with 5 km horizontal resolution at 850 hPa: PM_{2.5} concentration at (a) 1800 LT on October 24, 2016; (b) 2200 LT on October 24, 2016; and (c) 0800 LT on October 25, 2016.

of the PBL causing an increase in the concentration of PM₁₀ and PM_{2.5}. Those high concentrations measured by CETESB stations for this episode must be related not only with the traffic emissions and industrial activities but also with the biomass burning activity that happens during the dry season in the interior of SP state and also in the Amazonian basin and Central Brazil.

The results presented for July 10–13 are consistent with previous studies that show impact of the long-range transport of biomass burning on air quality in Southeast Brazil (Pickering et al., 1996; Hart and Spinaia, 1999; Freitas et al., 2005, 2009; Silva Dias, 2006; Rosário et al., 2013; De Oliveira et al., 2016; Martins et al., 2018), and the state of SP (Andrade et al., 2015, 2017; Kumar et al., 2016). However, within MASP the main sources of anthropogenic emissions remain industrial and traffic (Andrade et al., 2017; Vara-Vela et al., 2016; Ibarra-Espinosa et al., 2018). According to EDGAR emissions used for this work, for the MASP the combustion in the manufacturing industry (SNAP 03) are major emitters of PM₁₀ (89% of total emission of PM₁₀), and of PM_{2.5} with 40% of the total emission of PM_{2.5} in the MASP, while road transport (SNAP 07) with others mobile sources and machinery (SNAP 08) are responsible for 38% of total PM_{2.5} emissions (more information about emission per sector in the supplementary material Table S2). The model results show the complex vertical structure of PM concentrations over MASP enabling to distinguish PM from these two main source regions. In addition, it is noted that for these days the concentrations exceeded the threshold of PM₁₀ of daily 50 µg/m³ established by WHO. The maximum concentration occurred in C – MASP North on July 13 at 2200 LT, with a measured average concentration of PM₁₀ of 147 µg/m³ while EURAD – MASP North calculated 64 µg/m³.

In all cluster inter-comparisons for this episode in July the EURAD-IM simulations under-estimate the measured values in many cases by the order of 10–40%, especially when local concentration maxima occur. However, large differences between the measured concentration at individual sites within the clusters can also be observed in NW PAULÍNIA, NW CAMPINAS, NW LIMEIRA, Fig. 7d–f, respectively. The EURAD-IM model is not optimized for inner city air quality, as its regional scale is not representative comparing to individual monitoring stations within the city. Therefore, short concentration peaks produced by very local emissions cannot be reproduced by EURAD-IM. The

EDGAR emissions, since they are based on the year 2012, use emission factors based on international statistics in their estimates (IPCC, 2006a). The EDGAR inventory needs to be updated and improved. For the MASP, Ibarra-Espinosa et al. (2018), showed that VEIN estimates for CO were more than 20 times higher than corresponding EDGAR emissions, showing that EDGAR may underestimate PM₁₀ and PM_{2.5} as well.

3.2. Case study on October 22–25, 2016: transition season from dry winter to wet summer in southeastern Brazil

As a second study, PM concentrations in the period of October 22–25 are analyzed. The predominant synoptic situation during this second event is more complex than during the first event (Fig. 8). Fig. 8 shows the wind at 850 hPa and sea level pressure causing atmospheric stability on the Southeast, especially over SP, on 23 and 24 October. This stability is caused by the high-pressure system acting over the Atlantic Ocean reaching 1030 hPa over the Atlantic Ocean. The synoptic conditions were associated with another low-pressure system of 998 hPa, over Bolivia and a high-pressure system of 1030 hPa over the south and southeast coast and remained there for these days. During October 23–24, the weather situation over the state of SP is calm and stable. In general, higher pollutant concentrations can be observed in the presence of the high-pressure system, with stagnation of air circulation and more stable atmospheric conditions. The low-pressure system further South-west is responsible for atmospheric disturbances on October 25 causing instability over SP state. According to data from the National Institute of Meteorology (INMET, 2016) it rained over the MASP on October 25.

Fig. 9 presents AOD (Levy et al., 2013; Sayer et al., 2017), MODIS fire hotspots and thermal anomalies from Terra (MOD14) and Aqua (MYD14) for October 24 and 25, 2016, and vertical aerosol backscatter coefficients for 355 nm and 532 nm profiles for October 24, 2016. On October 24 and 25 (Fig. 9a and b) the atmosphere was cloudy over the MASP. Between 10:30 and 11:30 LT, the backscatter profile retrieved by the SPU-Lidar station presents three different aerosol layers. The first one, with a backscatter peak of 0.004 km⁻¹sr⁻¹, is due to the aerosol particulate trapped inside the PBL. The second one is an aerosol layer detached from the PBL, with a strong and sharp peak of 0.003 km⁻¹sr⁻¹

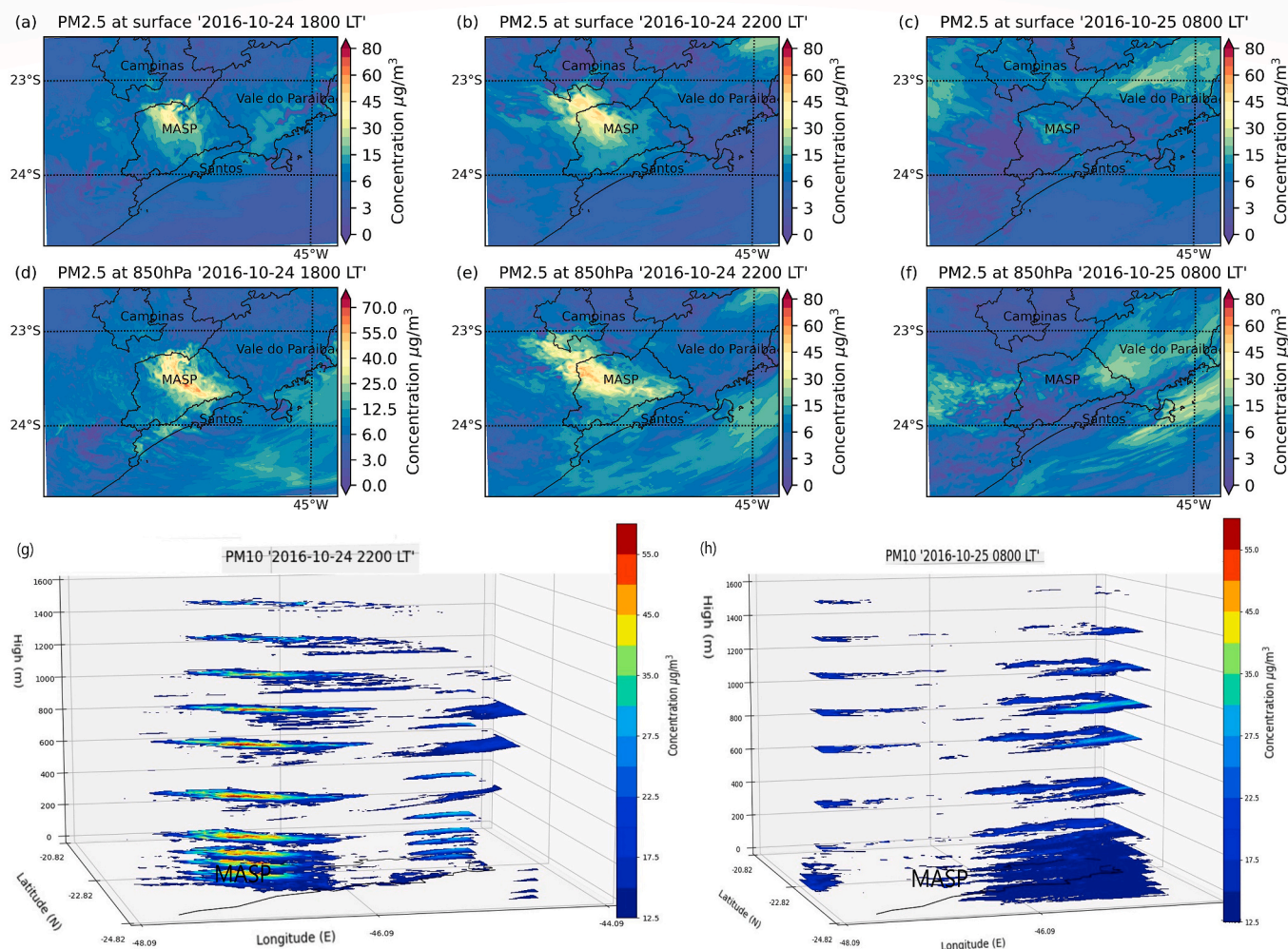


Fig. 11. PM_{2.5} concentration simulated by EURAD-IM on the 1-km domain at surface on October 24, 2016, 1800 LT (a); 2200 LT (b) and on October 25, 2016, 0800 LT (c). PM_{2.5} concentration simulated by EURAD-IM on the 1-km domain at 850 hPa on October 24, 2016, 1800 LT (d); 2200 LT (e) and on October 25, 2016, 0800 LT (f). PM_{2.5} concentrations on October 24, at 2200 LT (g) and October 25, at 0800 LT (h), 2016 for the lowest 10 levels of the model.

at 1440 m a.g.l., which can be associated with the intrusion of polluted air into MASP. The third aerosol layer detected is located between 2300 and 3700 m a.g.l. and also, due to the altitude range, can be associated to aerosol transported from long-range distances to MASP. For this case the total column Lidar ratio at 532 nm is 83 sr and can be associated to absorbing particles from biomass-burning (Weitkamp, 2005). The meteorological condition for October 24 shows stable atmospheric conditions which are favorable to pollutant accumulation. At 850 hPa the wind is coming from several direction reaching the MASP between October 22–25 (Fig. 8).

Fig. 10 shows simulated PM_{2.5} concentrations at 850 hPa on a 5 km horizontal resolution on October 24 at 1800 and at 2200 LT (Fig. 10a and b), as well as on October 25 at 0400 and 0800 LT (Fig. 10c and d). These times were chosen because they best represent the PM_{2.5} transport at 850 hPa level (simulations of PM_{2.5} and PM₁₀ for October 22, at 0400 LT to October 25, 1200 LT at 850 hPa for 1 km resolution are shown in Fig. S3 and Fig. S4). Especially on October 25, the pollution transported between MASP and MARJ (429 km distance) via the Paraíba Valley is clearly visible. Concentrations of over 25 µg/m³ are observed over the MASP on October 24 at 1800 LT and at 2200 LT at 850 hPa. This pollution is generated for the most part by evening rush hour and industries. Even with the high-pressure system affecting the atmospheric dynamics of the region (Fig. 8) it is possible to see that pollution is transported between the MASP and MARJ not only through the coast via the sea-breeze, but also through the Paraíba Valley. EURAD-IM

simulations show that pollutant transport in coastal regions such as S-Coast and MARJ are highly influenced by the dynamics of sea breezes and land breezes in these regions.

Fig. 11 shows the PM_{2.5} concentrations on the 1-km model domain at surface for October 24 at 1800 LT, and 2200LT, and for October 25 at 0800 LT. As expected, the high-resolution grid shows a higher PM concentration over the MASP mainly caused by vehicular emissions during the evening rush hours at around 1800 LT (Fig. 11a), as well as by industrial activities. Fig. 11 also shows the transport of PM_{2.5} from MARJ to MASP with concentrations of over 20 µg/m³ at 850 hPa on October 24, both at 1800 LT and 2200 LT via the coast, transported by the sea-breeze over the Atlantic and entering through the coast of Santos City into the direction of MASP. Also, a particle loaded air mass is coming through the Paraíba Valley from Rio de Janeiro in the direction of MASP. A similar behavior can be seen for PM₁₀ (Fig. S4).

At 850 hPa, with predominant wind direction east-northeast at Paraíba Valley and the coastal region of Santos (Fig. 8c and d), we faced the inverted situation than in the prior case study. For this reason, we calculated how much the PM₁₀ and PM_{2.5} plumes at 850 hPa contributed to the total PM₁₀ and PM_{2.5} concentration over MASP. We estimated that 26% of the total PM₁₀ and 28% of the total PM_{2.5} at 850 hPa at MASP are coming from Vale do Paraíba in October 24–25, while Santos contributed with 24% of the total PM₁₀ and 34% of the total PM_{2.5}. These results together with the analyzed meteorological data, show that the air pollution plumes from MASP and MARJ interact with

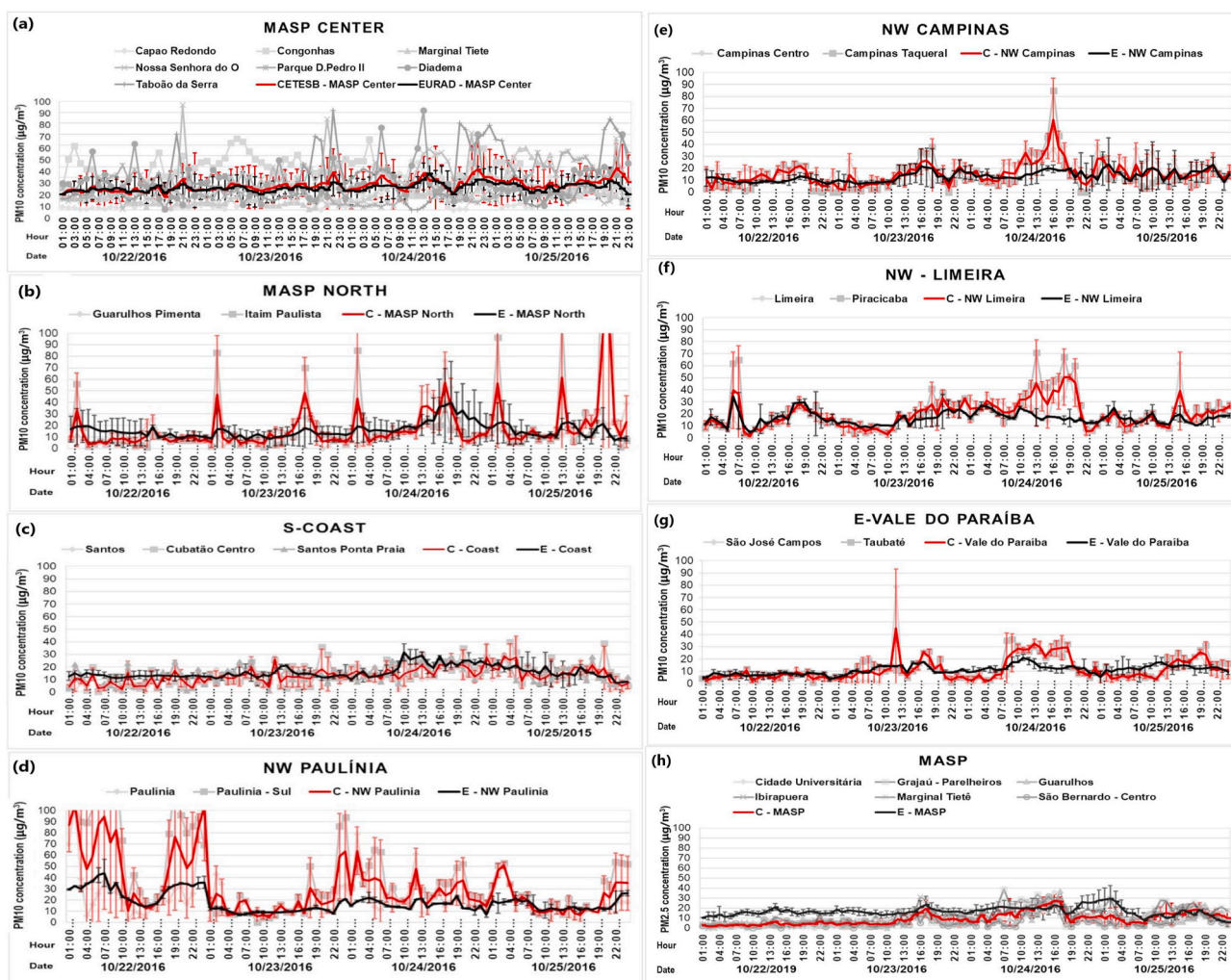


Fig. 12. PM10 concentrations for October 22–25, 2016 measured by CETESB stations and modeled by EURAD-IM. For each CETESB super-observation (red) the original data at the observation sites (grey) and EURAD-IM super-observation (black) are given. Table S1 defines the cluster grouping.

Table 3

Model quality indicators calculated with hourly concentration observed/ modeled on October 22–25, in 26 background sites (20 PM10 and 5 PM2.5 measurement sites) grouping in 8 clusters according to Table S1.

Cluster Name	r	RMSE	Bias
MASP Center (PM10)	0.75	3.53	−7.50
MASP North (PM10)	0.34	17.36	−8.70
NW Paulínia (PM10)	0.86	21.52	−41.90
NW Campinas (PM10)	0.61	7.40	−14.80
NW Limeira (PM10)	0.59	9.38	−17.20
S-Coast (PM10)	0.53	5.88	18.30
E-Vale do Paraíba (PM10)	0.60	7.21	−2.90
MASP (PM2.5)	0.35	9.47	76.40

each other depending on the meteorological conditions via two possible routes: via the Paraíba Valley and via the Rio de Janeiro/São Paulo coast. Freitas et al. (2007a) studied the meteorological conditions that favor these pollutants transport such as large-scale circulation in central-south-southeast region of Brazil, low- and high-pressure zones and local circulations such as sea breeze propagation, a factor that determines the dispersion of pollutants over MASP. Another important forcing is the complex topography of the region that can generate mountain-valley circulations mainly in the eastern and northwestern portions of MASP, between the Serra da Mantiqueira and the Paraíba Valley (Freitas et al., 2007a). The Urban Heat Island (UHI) is another

forcing that impact the local circulation and is provoked by the effect of urbanization and by human activities in MASP and MARJ.

The abrupt change in PM10 and PM2.5 concentrations between October 24 to 25 is due to late rain on October 24 in MASP, while in the MARJ the conditions remained dry according to meteorological data from the INMET (2016). Figs. 11g and h show PM2.5 concentrations for the lowest 10 levels of the model, showing the complex vertical structure of PM distribution. Fig. 11g shows a strong vertical mixing above MASP indicating the presence of an Urban Heat Island (UHI), a common meteorological phenomenon first studied over the MASP by Freitas et al. (2007a), who concluded that the UHI forms a strong convergence zone in the center of the city and thereby accelerates the sea-breeze front toward the city center.

Fig. 12 compares the modeled and observed PM10 and PM2.5 times series for October 22–25 clustered according to Table S1 and Table 3 presents statistical indexes for PM10 and PM2.5 for the October case study. For this second case study the datasets remain with the Pearson coefficient mostly varying between 0.50 and 0.70 for PM10, with the exception of NW PAULÍNIA with a correlation coefficient of 0.87, which constitutes a fairly strong positive relationship. Although the EURAD-IM simulation involves anthropogenic emissions, it is necessary to improve the emissions inventories to provide an as accurate as possible and consistent image of the atmosphere state at a given time. The vehicle, industrial and agricultural emissions scenario needs to be better defined for the region. The EURAD-IM performs well in MASP Center that

contains more observational sites and thus more representative standard deviations could be calculated. Model and observations agree within the error range (Fig. 12a). For the clusters MASP CENTER, S-Coast, NW PAULÍNIA, NW CAMPINAS and NW LIMEIRA (Figs. 12a and 12c–f), EURAD-IM simulations were inside the standard deviations of the observations with RMSE = 3.53 (Table 3). EURAD underestimates concentrations at MASP CENTER, MASP North, NW PAULÍNIA, NW CAMPINAS, NW LIMEIRA, E-Vale do Paraíba and overestimate at S-Coast. For PM_{2.5} concentrations at MASP CENTER the model did not show a good performance with a Pearson coefficient of $r = 0.35$ overestimating the observations by $76 \mu\text{g}/\text{m}^3$. The PM₁₀ concentration for October 22–25 was lower than during July 10–13 possibly related to the transition seasons and onset of the wet season during this month. These results also show that EURAD-IM requires more concise emission estimates to quantitatively reproduce the atmospheric state. The quality of results obtained is directly related to the quality and detail of the underlying atmospheric emission inventory of the region. Regarding Brazil, only very few cities have detailed inventories, and the use of global inventories is thus often unavoidable. Also, EURAD-IM is a mesoscale-alpha regional model working on a maximum horizontal resolution of 1 km and therefore steep and abrupt changes in vertical surface structure, typical for urban environments, cannot be resolved.

Differences in concentrations can reach more than $95 \mu\text{g}/\text{m}^3$: average concentrations of the C – MASP NORTH cluster on October 25 at 2100 LT were $118 \mu\text{g}/\text{m}^3$, while the model's average E – MASP North reached only $21 \mu\text{g}/\text{m}^3$. Other high PM₁₀ concentrations occurred on October 22 at C–NW Paulínia cluster, reaching a maximum concentration of $105 \mu\text{g}/\text{m}^3$, while the average model concentration at E – NW Paulínia was $44 \mu\text{g}/\text{m}^3$.

4. Conclusions

The mechanisms of elevated air pollution in the MASP have been studied by a novel modeling approach, resting on (i) a multiscale and multi-resolution model configuration, encompassing the MASP by a 25 km resolution domain over most part of South America, a 5 km domain over the Southeast Brazil and 1 km domain centered over the MASP and (ii) two weather situations prone to air quality decline. The first case study was set during the dry season of July 2016, one of the months marked by frequent annual episodes of long-range and regional pollution transport. The EURAD-IM elucidates well the role of the SALLJ in this long-range transport of PM from the center of South America and the local transport within SP state deteriorating the air quality of MASP. This pollution reaches the MASP and is also transported from the MASP following the northeastern direction through the Paraíba Valley and Atlantic coast, which is divided by the *Serra do Mar* (sea mountains) to Rio de Janeiro. The model reproduces the behavior of observed PM₁₀ concentrations but underestimated the observations, although it presents a Pearson coefficient $r > 0.7$ for the cluster in MASP Center. The second case study occurred from October 22–25, 2016, which is the transition season from dry winter to wet summer in southeastern Brazil. EURAD-IM simulations show that the air pollution from MASP and MARJ interact with each other depending on the meteorological conditions via two possible routes: via the Paraíba Valley or via the Rio de Janeiro/São Paulo coast. In both case studies, EURAD-IM results demonstrated that there can be exchange of pollutants between MASP and MARJ. In general, the model somewhat underestimates the observations which is explained by the scale of the model (1 km domain, as highest resolution) and the representativity of surface local observations in a highly variable chemical regime. These results also show that EURAD-IM requires better emissions inventories to reproduce an atmospheric state closer to the real state, as the vehicular, industrial and agricultural emissions from EDGAR do not represent well the PM_{2.5} emissions. The results and their limits clearly indicate that further detailed analyses of air quality conditions of the state of SP would highly benefit from a denser observation network, especially outside the city,

which also measures fine particulate matter (PM_{2.5}). As a next step, sensitivity tests will be performed including a high-resolution vehicular emission inventory for MASP and Brazil and make use of the 4D-Var assimilation system that is part of EURAD-IM to optimize the model results by assimilating heterogeneous in-situ and remote sensing observational data.

Credit author statement

Ediclê De Souza Fernandes Duarte: Conceptualization, Methodology, Validation, Formal analysis, Writing, Visualization. Philipp Franke: Software, Resources, Writing – review & editing, Supervision. Anne Caroline Lange: Software, Resources, Writing – review & editing, Supervision. Elmar Friese: Software, Resources. Fábio Juliano da Silva Lopes: Validation, Formal analysis, Resources, Data curation, Writing – review & editing, Visualization. Jonatan João da Silva: Data curation. Eduardo Landulfo: Resources., Cláudio Moises Santos e Silva: Supervision, Hendrik Elbern: Conceptualization, Methodology, Resources, Writing, Supervision, Project administration. Judith Johanna Hoelzemann: Conceptualization, Methodology, Validation, Formal analysis, Validation, Resources, Writing, Visualization, Supervision, Project administration.

Declaration of competing interest

The authors declare that they have no known competing financial interests or personal relationships that could have appeared to influence the work reported in this paper.

Acknowledgements

We thank the *Rheinisches Institut für Umweltforschung an der Universität zu Köln*, Germany for their continuous support and for hosting Ediclê Duarte during his 12 months research visit in 2018/2019, together with Research Center Jülich. The authors gratefully acknowledge the computing time granted through JARA on the supercomputer JURECA at *Forschungszentrum Jülich (Jülich Supercomputing Centre, 2018)*. This study was financed in part by the *Coordenação de Aperfeiçoamento de Pessoal de Nível Superior - Brazil (CAPES) - Finance Code 001*, Brazil, for the doctoral scholarship granted. São Paulo State Environmental Sanitation Technology Company (CETESB, Environmental Protection Agency) for the PM data. This article and the research behind it are a direct contribution to the research themes of the Klimapolis Laboratory (klimapolis.net). Networking and coordination activities of the Klimapolis Laboratory are funded by the German Federal Ministry of Education and Research (BMBF).

Appendix A. Supplementary data

Supplementary data related to this article can be found at <http://doi.org/10.1016/j.apr.2020.12.006>.

References

- Ackermann, I.J., 1997. MADE: entwicklung und Anwendung eines Aerosol-Dynamik modells für dreidimensionale Chemie-Transport-Simulationen in der Troposphäre, Ph.D. Thesis. Institut für Geophysik und Meteorologie der Universität zu Köln.
- Ackermann, I.J., Hass, H., Memmesheimer, M., Ebel, A., Binkowski, F.S., Shankar, U., 1998. Modal aerosol dynamics model for europe: development and first applications. *Atmos. Environ.* 32, 2981–2999.
- Albuquerque, T.T., Andrade, M.F., Ynoue, R.Y., 2012. Characterization of atmospheric aerosols in the city of São Paulo, Brazil: comparisons between polluted and unpolluted periods. *Environ. Monit. Assess.* <https://doi.org/10.1007/s10661-011-2013-y>.
- Albuquerque, T.T.A., Andrade, M.F., Ynoue, R.Y., Moreira, D.M., Andreão, W.L., Santos, F.S., Nascimento, E.G.S., 2018. WRF-SMOKE-CMAQ modeling system for air quality evaluation in São Paulo megacity with a 2008 experimental campaign data. *Environ. Sci. Pollut. Control Ser.* <https://doi.org/10.1007/s11356-018-3583-9>.

- Albuquerque, T.T.A., West, J., Andrade, M.F., Ynoue, R.Y., Andreão, W.L., Santos, F.S., Maciel, F.M., Pedruzzi, R., Mateus, V.O., Martins, J.A., Martins, L.D., Nascimento, E. G.S., Moreira, D.M., 2019. Analysis of PM_{2.5} concentrations under pollutant emission control strategies in the metropolitan area of São Paulo, Brazil. *Environmental Science and Pollution Research*. <https://doi.org/10.1007/s11356-019-06447-6>.
- Aleksankina, K., Reis, S., Vieno, M., Heal, M.R., 2019. Advanced methods for uncertainty assessment and global sensitivity analysis of a Eulerian atmospheric chemistry transport model. *Atmos. Chem. Phys.* <https://doi.org/10.5194/acp-19-2881-2019>.
- Allen, A.G., McGonigle, A.J.S., Cardoso, A.A., Machado, C.M.D., Davison, B., Paterlini, W.C., Rocha, G.O., Andrade, J.B., 2009. Influence of sources and meteorology on surface concentrations of gases and aerosols in a coastal industrial complex. *J. Braz. Chem. Soc.* 20, 214e221. <https://doi.org/10.1590/S0103-50532009000200004>.
- Alonso, M.F., Longo, K., Freitas, S., Fonseca, R., Marécal, V., Pirre, M., Klenner, L., 2010. An urban emission inventory for South America and its application in numerical modeling of atmospheric chemical composition at local and regional scales. *Atmospheric Environment*. <https://doi.org/10.1016/j.atmosenv.2010.09.013>.
- Andrade, M.F., Miranda, R.M., Fornaro, A., Kerr, A., Oyama, B., Andre, P.A., Saldiva, P., 2012. Vehicle emissions and PM_{2.5} mass concentrations in six Brazilian cities. *Air Quality, Atmosphere & Health*. <https://doi.org/10.1007/s11869-010-0104-5>.
- Andrade, M.F., Ynoue, R.Y., Freitas, E.D., Todesco, E., Vara Vela, A., Ibarra, S., Martins, L.D., Martins, J.A., Carvalho, V.S.B., 2015. Air quality forecasting system for southeastern Brazil. *Frontiers in Environmental Science*. <https://doi.org/10.3389/fenvs.2015.00009>.
- Andrade, M.F., Kumar, P., Freitas, E.D., Ynoue, R.Y., Martins, J., Martins, L.D., Nogueira, T., Perez-Martinez, P., Miranda, R.M., Albuquerque, T.T.A., Gonçalves, F.L.T., Oyama, B., Zhang, Y., 2017. Air Quality in the Megacity of São Paulo: Evolution over the Last 30 Years and Future Perspectives. *Atmospheric Environment*. <https://doi.org/10.1016/j.atmosenv.2017.03.051>.
- Andrae, M.O., Merlet, P., 2001. Emission of Trace Gases and Aerosols from Biomass Burning, Global Biogeochemical Cycles. <https://doi.org/10.1029/2000GB001382>.
- Andreão, W.L., Albuquerque, T.T.A., Kumar, P., 2018. Excess Deaths Associated with Fine Particulate Matter in Brazilian Cities. *Atmospheric Environment*. <https://doi.org/10.1016/j.atmosenv.2018.09.034>.
- Andreão, W.L., Alonso, M.F., Pinto, J.A., Pedruzzi, R., Albuquerque, T.T.A., 2020. Top Down Vehicle Emission Inventory for spatial distribution and dispersion modeling of particulate matter. *Environ. Sci. Pollut. Control Ser.* <https://doi.org/10.1007/s11356-020-08476-y>.
- Andreão, W.L., Pinto, J.A., Pedruzzi, R., Kumar, P., Albuquerque, T.T.A., 2020. Quantifying the impact of particle matter on mortality and hospitalizations in four Brazilian metropolitan areas. *J. Environ. Manag.* <https://doi.org/10.1016/j.jenvman.2020.110840>.
- Arakawa A., Lamb V. R. Computational design for the basic dynamical processes of UCLA general circulation model. *J. Comput. Phys.* <https://doi.org/10.1016/B978-0-12-460817-7.50009-4>.
- Artaxo, P., Fernandes, E.T., Martins, J.V., Yamasoe, M.A., Hobbs, P.V., Maenhaut, W., Longo, K.M., Castanho, A., 1998. Large scale Aerosol source apportionment in amazonia. *J. Geophys. Res.* 103 (D24), 31, 837-31.848.
- Artaxo, P., Andreae, M.O., Guenther, A., Rosenfeld, D., 2001. LBA Atmospheric Chemistry: unveiling the lively interactions between the biosphere and the Amazonian atmosphere. *IGBP Global Change Newsletter*. LBA Special Issue, pp. 12–15.
- Artaxo, P.V.G., Gatti, A.M.C., Leal, K.M., Longo, S.R., Freitas, L.L., Lara, T.M., Pauliquevis, A.S., Procópio, Rizzo L.V., 2005. Química atmosférica na Amazônia: a floresta e as emissões de queimadas controlando a composição da atmosfera amazônica. *Acta Amazonica*. <https://doi.org/10.1590/S0044-59672005000200008>.
- Asmi, E., Matti, A., Tarja, Y., Matti, J., Päivi, A., Timo, M., Risto, H., Kaarle, H., 2009. Driver and passenger exposure to aerosol particles in buses and trams in Helsinki, Finland. *Science of The Total Environment*. <https://doi.org/10.1016/j.scitotenv.2009.01.004>.
- Bahreini, R., Ahmadov, R., McKeen, S., Vu, K., Dingle, J., Apel, E., 2018. Sources and characteristics of summertime organic aerosol in the Colorado front range: perspective from measurements and WRF-chem modeling. *Atmos. Chem. Phys.* <https://doi.org/10.5194/acp-2018-57>.
- Benedetti, A., Morcrette, J.J., Boucher, O., Dethof, A., Engelen, R.J., Fisher, M., Flentje, H., Huneeus, N., Jones, L., Kaiser, J.W., Kinne, S., Mangold, A., Razinger, M., Simmons, A.J., Suttie, M., the GEMS-AER team, 2009. Aerosol analysis and forecast in the European Centre for medium-range weather forecasts integrated forecast system: data assimilation. *J. Geophys. Res.* <https://doi.org/10.1029/2008JD011115>.
- Binkowski, F.S., Shankar, U., 1995. The regional particulate matter model 1. Model description and preliminary results. *J. Geophys. Res.* <https://doi.org/10.1029/95JD02093>.
- Boldo, E., Linares, C., Aragonés, N., Lumbreras, J., Borge, R., De La Paz, D., Pérez-Gómez, B., Fernández-Navarro, P., García-Pérez, J., Pollán, M., Ramis, R., Moreno, T., Karanasiou, A., López-Abente, G., 2014. Air quality Modeling and mortality impact of fine particles reduction policies in Spain. *Environ. Res.* <https://doi.org/10.1016/j.envres.2013.10.009>.
- Campbell, P., Zhang, Y., Yan, F., Lu, Z., Streets, D., 2018. Impacts of transportation sector emissions on future U.S. air quality in a changing climate. Part I: projected emissions, simulation design, and model evaluation. *Environ. Pollut.* <https://doi.org/10.1016/j.envpol.2018.04.020>.
- Capucim, M.N., Brand, V.S., Machado, C.B., Martins, L.D., Allasia, D.G., Homann, C.T., Freitas, E.D., Silva, D., Andrade, M.F., Martins, J.A., 2015. South America land use and land cover assessment and preliminary analysis of their impacts on regional atmospheric modeling studies. *IEEE Journal of Selected Topics in Applied Earth Observations and Remote Sensing*. <https://doi.org/10.1109/JSTARS.2014.2363368>.
- Carvalho, V.S.B., Freitas, E.D., Martins, L.D., Martins, J.A., Mazzoli, C.R., Andrade, M.F., 2015. Air quality status and trends over the Metropolitan Area of São Paulo, Brazil as a result of emission control policies. *Environ. Sci. Pol.* <https://doi.org/10.1016/j.envsci.2014.11.001>.
- CETESB Relatório de Qualidade do ar no estado de São Paulo, 2009. Companhia Ambiental do Estado de São Paulo. São Paulo State Environmental Protection Agency. <http://ar.cetesb.sp.gov.br/publicacoes-relatorios/>. (Accessed 13 June 2019).
- CETESB Relatório de Qualidade do ar no estado de São Paulo, 2016. Companhia Ambiental do Estado de São Paulo. São Paulo State Environmental Protection Agency. <http://ar.cetesb.sp.gov.br/publicacoes-relatorios/>. (Accessed 13 June 2019).
- CETESB Relatório de Qualidade do ar no estado de São Paulo, 2017. Companhia Ambiental do Estado de São Paulo. São Paulo State Environmental Protection Agency. <http://ar.cetesb.sp.gov.br/publicacoes-relatorios/>. (Accessed 13 June 2019).
- Collet, S., Kidokoro, T., Karamchandani, P., Jung, J., Shah, T., 2018. Future year ozone source attribution modeling study using CMAQ-ISAM. *J. Air Waste Manag. Assoc.* <https://doi.org/10.1080/10962247.2018.1496954>.
- Cotton, W.R., Pielke, S.R.A., Walko, R.L., Liston, G.E., Tremback, C.J., Jiang, H., Mcanelly, R.L., Harrington, J.Y., Nicholls, M.E., Carrio, G.G., Mcfadden, J.P., 2003. RAMS 2001: current status and future directions. *Meteorol. Atmos. Phys.* <https://doi.org/10.1007/s00703-001-0584-9>.
- Crippa, M., Diego, G., Marilena, M., Edwin, S., Frank, D., John, A.A., Suvi, M., Ulrike, D., Jos, G.J.O., Valerio, P., 2018. Greet Janssens-Maenhout1 Gridded Emissions of Air Pollutants for the Period 1970-2012 within EDGAR v4.3.2. *Earth System Science Data*. <https://doi.org/10.5194/essd-2018-31>.
- Damian-Iordache, V., 1996. KPP - Chemistry Simulation Development Environment. Ph. D. Thesis. The University of Iowa, December, 1996.
- de Oliveira, A.M., Mariano, G.L., Alonso, M.F., Mariano, E.V.C., 2016b. Analysis of incoming biomass burning aerosol plumes over southern Brazil. *Atmos. Sci. Lett.* 17, 577–585.
- Ding, D., Zhu, Y., Jang, C., Lin, C.-J., Wang, S., Fu, J., Gao, J., Deng, S., Xie, J., Qiu, X., 2016. Evaluation of health benefit using BenMAP-CE with an integrated scheme of model and monitor data during Guangzhou Asian Games. *J. Environ. Sci.* <https://doi.org/10.1016/j.jes.2015.06.003>.
- IBGE, 2018. Diretoria de Pesquisas, Coordenação de População e Indicadores Sociais. 2018 e 2019 - estimativas das populações residentes municipais calculadas com base na Projeção da população para o Brasil e Unidades da Federação, por sexo e idade, Revisão. Notas metodológicas podem ser consultadas em. Accessed July 01, 2020. <https://www.ibge.gov.br/estatisticas/sociais/populacao/9103-estimativasdepopulacao.html?=&t=notastecnicas>.
- Dudhia, J., 1989. Numerical study of convection observed during the Winter Monsoon Experiment using a mesoscale two-dimensional model. *J. Atmos. Sci.* [https://doi.org/10.1175/1520-0469\(1989\)046<3077:NSOCOD>2.0.CO;2PDF](https://doi.org/10.1175/1520-0469(1989)046<3077:NSOCOD>2.0.CO;2PDF).
- Ebel, A., Elbern, H., Feldmann, H., Jakobs, H.J., Kessler, C., Memmesheimer, M., Oberreuter, A., Piekorz, G., 1997. Air Pollution Studies with the EURAD Model System, vol. 120. *Mitteilungen aus dem Institut für Geophysik und Meteorologie der Universität zu Köln*, 1997.
- Elbern, H., Schmidt, H., 2002. Chemical 4D variational data assimilation and its numerical implications for case study analyses. In: *IMA Volumes in Mathematics and its Applications*. Atmospheric Modeling. https://doi.org/10.1007/978-3-642-12535-5_24.
- Elbern, H., Schmidt, H., Talagrand, O., Ebel, A., 2000. 4D-variational Data Assimilation with an Adjoint Air Quality Model for Emission Analysis. *Environmental Modelling & Software*. [https://doi.org/10.1016/S1364-8152\(00\)00049-9](https://doi.org/10.1016/S1364-8152(00)00049-9).
- Elbern, H., Strunk, A., Schmidt, H., Talagrand, O., 2007. Emission rate and chemical state estimation by 4-dimensional variational inversion. *Atmos. Chem. Phys.* <https://doi.org/10.5194/acp-7-3749-2007>.
- Elbern, H., Schwinger, J., Botchorishvili, R., 2010. Chemical state estimation for the middle atmosphere by four-dimensional variational data assimilation: system configuration. *J. Geophys. Res.* <https://doi.org/10.1029/2009JD011953>.
- Eurostat, 2004. *NAMEA for Air Emissions Compilation Guide* (Luxembourg, Eurostat. [Google Scholar]).
- Faiz, A., Weaver, C.S., Walsh, M.P., 1996. Air Pollution from Motor Vehicles: Standards and Technologies for Controlling Emissions. <https://doi.org/10.1596/0-8213-3444-1>. Published: November 1996, ISBN: 978-0-8213-3444-7.
- Flemming, J., Huijnen, V., Arteta, J., Bechtold, P., Beljaars, A., Blechschmidt, A.-M., Diamantakis, M., Engelen, R.J., Gaudel, A., Inness, A., Jones, L., Josse, B., Katragkou, E., Marecal, V., Peuch, V.-H., Richter, A., Schultz, M.G., Stein, O., Tsikerdekis, A., 2015. Tropospheric chemistry in the integrated forecasting system of ECMWF. *Geoscientific Model Development*. <https://doi.org/10.5194/gmd-8-975-2015>.
- Freitas, S.R., Longo, K.M., Silva Dias, M.A.F., Silva Dias, P.L., Chatfield, R., Prins, E., Recuero, F.S., 2005. Monitoring the transport of biomass burning emissions in South America. *Environ. Fluid Mech.* 5, 135–167.
- Freitas, E.D., Rozoff, C.M., Cotton, W.R., Silva Dias, P.L., 2007a. Interactions of an urban heat island and sea breeze circulations during winter over the Metropolitan Area of São Paulo - Brazil. *Boundary-Layer Meteorol.* <https://doi.org/10.1007/s10546-006-9091-3>.
- Freitas, E.D., Martins, L.D., Mazzoli, C.R., Martins, J.A., Hallak, R., Itimura, M.S., Carvalho, V.S.B., Silva Dias, P.L., Andrade, M.F., 2007b. Particulate matter concentration forecast over the metropolitan area of São Paulo. *Cienc. Nat.* <https://doi.org/10.5902/2179460X9914>.

- Freitas, S.R., Longo, K.M., Chatfield, R., Latham, D., Silva Dias, M.A.F., Andreae, M.O., Prins, E., Santos, J.C., Gielow, R., Carvalho, J.J.A., 2007c. Including the sub-grid scale plume rise of vegetation fires in low resolution atmospheric transport models. *Atmos. Chem. Phys.* <https://doi.org/10.5194/acp-7-3385-2007>.
- Freitas, S.R., Longo, K.M., Silva Dias, M.A.F., Chatfield, R., Silva Dias, P., Artaxo, P., Artaxo, M.O., Grell, G., Rodrigues, L.F., Fazenda, A., Panetta, J., 2009. The coupled aerosol and tracer transport model for the Brazilian developments on the regional atmospheric modeling system (CATT-BRAMS) – Part 1: model description and evaluation. *Atmos. Chem. Phys.* 9, 2843–2861. <https://doi.org/10.5194/acp-9-2843-2009>.
- Freitas, S.R., Panetta, J., Longo, K.M., Rodrigues, L.F., Moreira, D.S., Rosario, N.E., Silva Dias, P.L., Silva Dias, M.A.F., Souza, E.P., Freitas, E.D., Longo, M., Frasson, A., Fazenda, A.L., Santos, E., Silva, C.M., Pavani, C.A.B., Eiras, D., Franca, D.A., Massaru, D., Silva, F.B., Santos, F.C., Pereira, G., Camponogara, G., Ferrada, G.A., Campos, H.F., Campos, V.H.F., Menezes, I., Freire, J.L., Alonso, M.F., Gacita, M.S., Zarzur, M., Fonseca, R.M., Lima, R.S., Siqueira, R.A., Braz, R., Tomita, S., Oliveira, V., Martins, L.D., 2017. The Brazilian developments on the Regional Atmospheric Modeling System (BRAMS 5.2): an integrated environmental model tuned for tropical areas. *Geoscientific Model Development*. <https://doi.org/10.5194/gmd-10-189-2017>.
- Gama, C., Ribeiro, I., Lange, A.C., Vogel, A., Ascenso, A., Seixas, V., Elbern, H., Borrego, H., Friese, E., Monteiro, A., 2019. Performance assessment of CHIMERE and EURAD-IM[†] dust modules. *Atmospheric Pollution Research*. <https://doi.org/10.1016/j.apr.2019.03.005>.
- Geiger, H., Barnes, I., Bejan, T., Benter, Spittler, M., 2003. The tropospheric degradation of isoprene: an updated module for the regional atmospheric chemistry mechanism. *Atmos. Environ.* [https://doi.org/10.1016/S1352-2310\(02\)01047-6](https://doi.org/10.1016/S1352-2310(02)01047-6).
- Granier, C., Bessagnet, B., Bond, T., D'Angiola, A., Denier van der Gon, H., Frost, G., Heil, A., Kaiser, J., Kinne, S., Klimont, Z., Kloster, S., Lamarque, J.-F., Liousse, C., Masui, T., Meleux, F., Mieville, A., Ohara, T., Raut, J.-C., Riahi, K., Schultz, M., Smith, S., Thompson, A., Aardenne, J., Werf, G., Vuuren, D., 2011. Evolution of anthropogenic and biomass burning emissions of air pollutants at global and regional scales during the 1980–2010 period. *Climatic Change*. <https://doi.org/10.1007/s10584-011-0154-1>.
- Grell, G.A., Freitas, S.R., 2014. A scale and aerosol aware stochastic convective parameterization for weather and air quality modeling. *Atmos. Chem. Phys.* 14, 5233–5250. <https://doi.org/10.5194/acp-14-5233-2014>.
- Grell, G.A., Peckham, S.E., Schmitz, R., McKeen, S.A., Frost, G., Skamarock, W.C., 2005. Fully coupled “online” chemistry within the WRF model. *Atmospheric Environment*. <https://doi.org/10.1016/j.atmosenv.2005.04.027>.
- Gulia, S., Shiva Nagendra, S.M., Khare, Mukesh, Khanna, Isha, 2015. Urban air quality management-A review. *Atmospheric Pollution Research*. <https://doi.org/10.5094/APR.2015.033>.
- Gurjar, B.R., Butler, T.M., Lawrence, M.G., Lelieveld, J., 2008. Evaluation of emissions and air quality in megacities. *Atmos. Environ.* <https://doi.org/10.1016/j.atmosenv.2007.10.048>.
- Hart, W., Spinfaiiae, J., 1999. Correlation between smoke and tropospheric ozone concentration in Cuiabá during Smoke, Clouds, and Radiation-Brazil (SCAR-B). *J. Geophys. Res.* 104, 12113–12129.
- Hass, H., 1991. Description of the EURAD Chemistry-Transport-Model Version 2 (CTM2), Vol 83. *Mitteilungen aus dem Institut für Geophysik und Meteorologie der Universität zu Köln*, 1991.
- Hoelzemann, J.J., Longo, K.M., Fonseca, R.M., Rosário, N.M.E., Elbern, H., Freitas, S.R., 2009. Regional representativity of AERONET observation sites in South America determined by correlation studies with MODIS Aerosol Optical Depth. *J. Geophys. Res.: Atmosphere*. <https://doi.org/10.1029/2008JD010369>.
- Hoesly, R.M., Smith, S.J., Feng, L., Klimont, Z., Janssens-Maenhout, G., Pitkanen, T., Seibert, J.J., Vu, L., Andres, R.J., Bolt, R.M., Bond, T.C., Dawidowski, L., Kholod, N., Kurokawa, J.I., Li, M., Liu, L., Lu, Z., Moura, M.C.P., O'Rourke, P.R., Zhang, Q., 2017. Historical (1750–2014) anthropogenic emissions of reactive gases and aerosols from the Community Emission Data System (CEDS). *Geoscientific Model Development*. <https://doi.org/10.5194/gmd-2017-43>.
- Hollingsworth, A., Engelen, R.J., Textor, C., Benedictti, A., Boucher, O., Chevallier, F., Dethof, A., Elbern, H., Eskes, H., Flemming, J., Granier, C., Kaiser, J.W., Morcrette, J. J., Rayner, R., Peuch, V.-H., Rouil, L., Schultz, M.G., Simmons, A.J., The, GEMS Consortium, 2008. Toward a monitoring and forecasting system for atmospheric composition: the GEMS project. *Bulletin of the American Meteorological Society*. <https://doi.org/10.1175/2008BAMS2355.1>.
- Hong, S.-Y., Dudhia, J., Chen, S.H., 2004. A revised approach to ice microphysical processes for the bulk parameterization of clouds and precipitation. *Mon. Weather Rev.* [https://doi.org/10.1175/1520-0493\(2004\)132<0103:ARATIM>2.0.CO;2](https://doi.org/10.1175/1520-0493(2004)132<0103:ARATIM>2.0.CO;2).
- Hong, S.-Y., Yign, N., Dudhia, J., 2006. A new vertical diffusion package with an explicit treatment of entrainment processes. *Mon. Weather Rev.* <https://doi.org/10.1175/MWR3199.1>.
- Hsu, N.C., Jeong, M.-J., Bettenhausen, C., Sayer, A.M., Hansell, R., Hansell, C.S., Huang, J., Tsay, S.-C., 2013. Enhanced Deep Blue aerosol retrieval algorithm: the second generation. *J. Geophys. Res. Atmos.* 118, 9296–9315. <https://doi.org/10.1002/jgrd.50712>.
- Hsu, N.C., Hsu, J., Sayer, A.M., Kim, W., Bettenhausen, C., Tsay, S.-C., 2019. VIIRS Deep Blue Aerosol Products over Land: Extending the EOS Long-Term Aerosol Data Records. <https://doi.org/10.1029/2018JD029688>.
- Huijnen, V., Williams, J., van Weele, M., van Noije, T., Krol, M., Dentener, F., Segers, A., Houweling, S., Peters, W., de Laat, J., Boersma, F., Bergamaschi, P., van Velthoven, P., Le Sager, P., Eskes, H., Alkemade, F., Scheele, R., Nédélec, P., Pätz, H.-W., 2010. The global chemistry transport model TM5: description and evaluation of the tropospheric chemistry version 3.0. *Geoscientific Model Development*. <https://doi.org/10.5194/gmd-3-445-2010>.
- Ibarra-Espinoza, S., Ynoue, R., O'Sullivan, S., Pebesma, E., Andrade, M.D.F., Osses, M., 2018. Vein v0.2.2: an r package for bottom-up vehicular emissions inventories. *Geoscientific Model Development*. <https://doi.org/10.5194/gmd-11-2209-2018>.
- IBGE, 2020. Available at: <https://mapas.ibge.gov.br/fisicos/estaduais>. (Accessed 17 May 2020).
- INMET, 2016. <http://www.inmet.gov.br/portal/>. (Accessed 15 May 2019).
- Inness, A., Ades, M., Agustí-Panareda, A., Barré, J., Benedictow, A., Blechschmidt, A.-M., Dominguez, J.J., Engelen, R., Eskes, H., Flemming, J., Huijnen, V., Jones, L., Kipling, Z., Massart, S., Parrington, M., Peuch, V.-H., Razinger, M., Remy, S., Schulz, M., Suttie, M., 2019. The CAMS reanalysis of atmospheric composition. *Atmos. Chem. Phys.* 19, 3515–3556. <https://doi.org/10.5194/acp-19-3515-2019>.
- INPE, 2016. Accessed July 01, 2020. <http://queimadas.dgi.inpe.br/queimadas/portal>.
- Janssens-Maenhout, G., Crippa, M., Guizzardi, D., Dentener, F., Muntean, M., Pouliot, G., Keating, T., Zhang, Q., Kurokawa, J., Wankmüller, R., Denier van der Gon, H., Kuenen, J.J.P., Klimont, Z., Frost, G., Darras, S., Koffi, B., Li, M., 2015. HTAP.v2.2: a mosaic of regional and global emission grid maps for 2008 and 2010 to study hemispheric transport of air pollution. *Atmos. Chem. Phys.* <https://doi.org/10.5194/acp-15-11411-2015>.
- Jiang, F., Liu, Q., Huang, X., Wang, T., Zhuang, B., Xie, M., 2012. Regional modeling of secondary organic aerosol over China using WRF/Chem. *J. Aerosol Sci.* <https://doi.org/10.1016/j.jaerosci.2011.09.003>.
- Jiang, N., Scorgie, Y., Hart, M., Riley, M.L., Crawford, J., Beggs, P.J., Edwards, G.C., Chang, L., Virgilio, G.D., 2017. Visualizing the relationships between synoptic circulation type and air quality in Sydney, a subtropical coastal-basin environment. *Int. J. Climatol.* <https://doi.org/10.1002/joc.4770>.
- Jülich Supercomputing Centre, 2018. JURECA: modular supercomputer at jülich supercomputing Centre. *Journal of large-scale research facilities* 4, A132. <https://doi.org/10.17815/jlsrf-4-121-1>.
- Kaiser, J.W., Heil, A., Andreae, M.O., Benedetti, A., Chubarova, N., Jones, L., Morcrette, J.-J., Razinger, M., Schultz, M.G., Suttie, M., van der Werf, G.R., 2012. Biomass burning emissions estimated with a global fire assimilation system based on observed fire radiative power. *Biogeosciences*. <https://doi.org/10.5194/bg-9-527-2012>.
- Klimont, Z., Kupiainen, K., Heyes, C., Purohit, P., Cofala, J., Rafaj, P., Borken-Kleefeld, J., Schöpp, W., 2017. Global anthropogenic emissions of particulate matter including black carbon. *Atmos. Chem. Phys.* <https://doi.org/10.5194/acp-17-8681-2017>.
- Kumar, P., Andrade, M.F.A., Ynoue, R.Y., Fornaro, A., Freitas, E.D., Martins, J., Martins, L.D., Albuquerque, T.T., Zhang, Y., Morawska, L., 2016. New directions: from biofuels to wood stoves: the modern and ancient air quality challenges in the megacity of São Paulo. *Atmos. Environ.* <https://doi.org/10.1016/j.atmosenv.2016.05.059>.
- Lanki, T., Vanninen, E., de Hartog, J., et al., 2006. Effects of ultrafine and fine particulate and gaseous air pollution on cardiac autonomic control in subjects with coronary artery disease: the ULTRA study. *J. Expo. Sci. Environ. Epidemiol.* 16, 332–341. <https://doi.org/10.1038/sj.jea.7500460>.
- Levy, R.C., Mattoo, S., Munchak, L.A., Remer, L.A., Sayer, A.M., Patadia, F., Hsu, N.C., 2013. The Collection 6 MODIS aerosol products over land and ocean. *Atmospheric Measurement Techniques*. <https://doi.org/10.5194/amt-6-2989-2013>.
- Li, J., Zhu, Y., Kelly, J.T., Jang, C.J., Wang, S., Hanna, A., Xing, J., Lin, C.-J., Long, S., Yu, L., 2019. Health benefit assessment of PM2.5 reduction in Pearl River Delta region of China using a model-monitor data fusion approach. *J. Environ. Manag.* <https://doi.org/10.1016/j.jenvman.2018.12.060>.
- Libonati, R., DaCamara, C.C., Setzer, A.W., Morelli, F., Melchiori, A.E., 2015. An algorithm for burned area detection in the Brazilian Cerrado using 4 µm MODIS imagery. *Rem. Sens.* <https://doi.org/10.3390/rs71115782>.
- Lin, L., Lee, M.L., Eatough, D.J., 2010. Review of recent advances in detection of organic markers in fine particulate matter and their use for source apportionment. *J. Air Waste Manag. Assoc.* <https://doi.org/10.3155/1047-3289.60.1.3>.
- Longo, K.M., Freitas, S.R., Andreae, M.O., Setzer, A., Prins, E., Artaxo, P., 2010. The coupled aerosol and tracer transport model to the Brazilian developments on the regional atmospheric modeling system (CATT-BRAMS) – Part 2: model sensitivity to the biomass burning inventories. *Atmos. Chem. Phys.* 10, 5785–5795. <https://doi.org/10.5194/acp-10-5785-2010>.
- Lowe, D., Archer-Nicholls, S., Morgan, W., Allan, J., Allan, S., Ouyang, B., Le Breton, E. M., Le Breton, R.A., Di Carlo, P., Percival, C., Coe, H., Jones, R., Jones, G., 2015. WRF-Chem model predictions of the regional impacts of N2O5 heterogeneous processes on night-time chemistry over north-western Europe. *Atmos. Chem. Phys.* <https://doi.org/10.5194/acp-15-1385-2015>.
- Marçal, V., Peuch, V.-H., Andersson, C., Andersson, S., Arteta, J., Beekmann, M., Benedictow, A., Bergström, R., Bessagnet, B., Cansado, A., Chéroux, F., Colette, A., Coman, A., Curier, R.L., Denier van der Gon, H.A.C., Drouin, A., Elbern, H., Emili, E., Engelen, R.J., Eskes, H.J., Foret, G., Friese, E., Gauss, M., Giannaros, C., Guth, J., Joly, M., Jaumouillé, E., Josse, B., Kadyrov, N., Kaiser, J.W., Krajsek, K., Kuenen, J., Kumar, U., Liora, N., Lopez, E., Malherbe, L., Martinez, I., Melas, D., Meleux, F., Menut, L., Moïnau, P., Morales, T., Parmentier, J., Piacentini, A., Plu, M., Poupkou, A., Queguiner, S., Robertson, L., Rouil, L., Schaap, M., Segers, A., Sofiev, M., Tarasson, L., Thomas, M., Timmermans, R., Valdebenito, A., van Velthoven, P., van Versendaal, R., Vira, J., Ung, A., 2015. A regional air quality forecasting system over Europe: the MACC-II daily ensemble production. *Geosci. Model Dev. (GMD)*. <https://doi.org/10.5194/gmd-8-2777-2015>, 2015.
- Marengo, J.A., Soares, W.R., Saulo, C., Nicolini, M., 2004. Climatology of the low-level jet east of the Andes as derived from the NCEP–NCAR reanalyses: characteristics and temporal variability. *J. Clim.* [https://doi.org/10.1175/1520-0442\(2004\)017<2261:COLTJE>2.0.CO;2](https://doi.org/10.1175/1520-0442(2004)017<2261:COLTJE>2.0.CO;2).

- Martins, L.D., Hallak, R., Alves, R.C., de Almeida, D.S., Squizzato, R., Moreira, C.A.B., Beal, A., Da Silva, I., Rudke, A., Martins, J.A., 2018. Long-range transport of aerosols from biomass burning over southeastern of South America and their implications on air quality. *Aerosol and Air Quality Research* 18, 1734. <https://doi.org/10.4209/aaqr.2017.11.0545>.
- Masson, V., 2000. A physically-based scheme for the urban energy budget in atmospheric models. *Boundary-Layer Meteorol.* <https://doi.org/10.1023/A:1002463829265>.
- McRae G. J., W. R. Goodin and J. H. Seinfeld, Numerical solution of the atmospheric diffusion equation for chemically reacting flows. *J. Comput. Phys.*, [https://doi.org/10.1016/0021-9991\(82\)90101-2](https://doi.org/10.1016/0021-9991(82)90101-2).
- Memmesheimer, M., Tippke, J., Ebel, A., Hass, H., Jakobs, H.J., Jakobs, M., 1991. On the use of EMEP emission inventories for European scale air pollution modelling with the EURAD model. In: Proceedings of the EMEP Workshop on Photooxidant Modelling for Long Range Transport in Relation to Abatement Strategies. https://doi.org/10.1007/978-3-662-03470-5_2.
- Memmesheimer, M., Jakobs, H.J., Feldmann, H., Feldmann, G., Feldmann, C., Ebel, A., 2000. Computergestützte Langzeitsimulationen zur Bewertung von Strategien zur Luftreinhaltung. Abschlussbericht zum Vorhaben COSIMA im Auftrag des Landesumweltamtes Nordrhein-Westfalen.
- Memmesheimer, M., Friese, E., Friese, A., Friese, H.J., Friese, H., Kessler, C., Piekorz, G., 2004. Long-term simulations of particulate matter in Europe on different scales using sequential nesting of a regional model. *Int. J. Environ. Pollut.* <https://doi.org/10.1504/IJEP.2004.005530>.
- Miranda, R.M., Andrade, M.F., Fornaro, A., Astolfo, R., Andre, P.A., Saldiva, P., 2012. Urban air pollution: a representative survey of PM_{2.5} mass concentrations in six Brazilian cities. *Air Quality, Atmosphere & Health*. <https://doi.org/10.1007/s11869-010-0124-1>.
- Miranda, R.M., Lopes, F., Rosário, N.É., Yamasoe, M.A., Landulfo, E., Andrade, M.F., 2017. The relationship between aerosol particles chemical composition and optical properties to identify the biomass burning contribution to fine particles concentration: a case study for São Paulo city, Brazil. *Environ. Monit. Assess.* <https://doi.org/10.1007/s10661-016-5659-7>.
- Mlawer, E.J., Taubman, S.J., Brown, P.D., Iacono, M.J., Clough, S.A., 1997. Radiative transfer for inhomogeneous atmospheres: RRTM, a validated correlated-*k* model for the longwave. *J. Geophys. Res.* <https://doi.org/10.1029/97JD00237>.
- Molina, L.T., Molina, M.J., 2002. *Air Quality in the Mexico Megacity: an Integrated Assessment*. Kluwer Academic Publishers, Dordrecht, The Netherlands, p. 384p.
- Molina, M.J., Molina, L.T., 2004. Megacities and atmospheric pollution. *J. Air Waste Manag. Assoc.* <https://doi.org/10.1080/10473289.2004.10470936>.
- Molina, L.T., Kolb, C.E., de Foy, B., Lamb, B.K., Brune, W.H., Jimenez, J.L., Ramos-Villegas, R., Sarmiento, J., Paramo, F.V.H., Cardenas, B., Gutierrez-Avedoy, V., Molina, M.J., 2007. Air quality in North America's most populous city – overview of the MCMA-2003 campaign. *Atmos. Chem. Phys.* <https://doi.org/10.5194/acp-7-2447-2007>.
- Monahan, E.C., 1988. *Coverage as a Remotely Monitorable Indication of the Rate of Bobbie Injection into the Oceanic Mixed Layer*. Springer Netherlands.
- Monteiro, A., Ribeiro, I., Tchepel, O., Sá, E., Ferreira, J., Carvalho, A., Martins, V., Strunk, A., Galmarini, S., Elbern, H., Schaap, M., Builtsjes, P., Miranda, A.I., Borrego, C., 2013. Bias correction techniques to improve air quality ensemble predictions: focus on O₃ and PM over Portugal. *Environ. Model. Assess.* <https://doi.org/10.1007/s10666-013-9358-2>, 2013.
- Morcrette, J.-J., Boucher, O., Jones, L., Salmond, D., Bechtold, P., Beljaars, A., Benedetti, A., Bonet, A., Kaiser, J.W., Razinger, M., Schulz, M., Serrari, S., Simmons, A.J., Sofiev, M., Suttie, M., Tompkins, A.M., Untch, A., 2009. Aerosol analysis and forecast in the European Centre for Medium-Range Weather Forecasts Integrated Forecast System: forward modeling. *J. Geophys. Res.* <https://doi.org/10.1029/2008JD011235>, 2009.
- Moreira, D.S., Freitas, S.R., Bonatti, J.P., Mercado, L.M., Rosario, N.M.E., Longo, K.M., Miller, J.B., Gloor, M., Gatti, L.V., 2013. Coupling between the JULES land-surface scheme and the CCATT-BRAMS atmospheric chemistry model (JULES-CCATT-BRAMS1.0): applications to numerical weather forecasting and the CO₂ budget in South America. *Geosci. Model Dev. Discuss. (GMDD)*. <https://doi.org/10.5194/gmdd-6-453-2013>.
- NASA (national aeronautics and space administration). source: <https://worldview.earthdata.nasa.gov/top%20July%2011%20and%2012%20respectively>. (Accessed 13 June 2020).
- Nogueira, E.M., Yanai, A.M., Fonseca, F.O.R., Fearnside, P.M., 2015. Carbon stock loss from deforestation through 2013 in Brazilian Amazonia. *Global Change Biol.* 21 (3), 1271–1292. <https://doi.org/10.1111/gcb.12798>.
- Pedruzzi, R., Baek, B.H., Henderson, B.H., Aravanis, N., Pinto, J.A., Araujo, I.B., Nascimento, E.G.S., Reis Junior, N.C., Moreira, D.M., Albuquerque, T.T.A., 2019. Performance evaluation of a photochemical model using different boundary conditions over the urban and industrialized metropolitan area of Vitoria, Brazil. *Environ. Sci. Pollut. Control Ser.* <https://doi.org/10.1007/s11356-019-04953-1>.
- Pickering, K.E., Thompson, A.M., Wang, Y., Tao, W.K., McNamara, D.P., Kirchner, V.W., J.H., Heikes, B.G., Sachse, G.W., Bradshaw, J.D., Gregory, G.L., Blake, D.R., 1996. Convective transport of biomass burning emissions over Brazil during TRACE A. *J. Geophys. Res.* 101, 23993–24012.
- Pielke, R.A., Cotton, W.R., Walko, L.R., Tremback, C.J., Lyons, W.A., Grasso, L.D., Nicholls, M.E., Moran, M.D., Wesley, D.A., Lee, T.J., Copeland, J.H., 1992. A comprehensive meteorological modeling system – RAMS, Meteorology and Atmospheric Physics. <https://doi.org/10.1007/BF01025401>.
- Pinto, J.A., Kumar, P., Alonso, M.F., Andrea, W.L., Pedruzzi, R., Santos, F.S., Moreira, D.M., Albuquerque, T.T.A., 2020. Traffic data in air quality modeling: a review of key variables, improvements in results, open problems and challenges in current research. *Atmospheric Pollution Research*. <https://doi.org/10.1016/j.apr.2019.11.018>.
- Pöschl, U., von Kuhlmann, R., Poisson, N., Crutzen, P.L., 2000. Development and intercomparison of condensed isoprene oxidation mechanisms for global atmospheric modeling. *J. Atmos. Chem.* <https://doi.org/10.1023/A:1006391009798>.
- Rafee, S.A.A., Kawashima, A.B., Morais, M.V.B., Urbina, V., Martins, L.D., Martins, J.A., 2015. Assessing the impact of using different land cover classification in regional modeling studies for the Manaus area, Brazil. *J. Geosci. Environ. Protect.* <https://doi.org/10.4236/gep.2015.36013>.
- Rafee, S.A.A., Martins, L.D., Kawashima, A.B., Almeida, D.S., Morais, M.V.B., Souza, R.V. A., Oliveira, M.B.L., Souza, R.A.F., Medeiros, A.S.S., Urbina, V., Freitas, E.D., Martin, S.T., Martins, J.A., 2017. Mobile and stationary sources of air pollutants in the Amazon rainforest: a numerical study with WRF-Chem model. *Atmos. Chem. Phys.* <https://doi.org/10.5194/acp-2016-1190>.
- Ring, A.M.M., Canty, T.P., Anderson, D.C., Vinciguerra, T.P., He, H., Goldberg, D.L., Ehrman, S.H., Dickerson, R.R., Salawitch, R.J., 2018. Evaluating commercial marine emissions and their role in air quality policy using observations and the CMAQ model. *Atmospheric Environment*. <https://doi.org/10.1016/j.atmosenv.2017.10.037>.
- Rodrigues, J.A., Libonati, R., Pereira, A.A., Nogueira, J.M.P., Santos, F.L.M., Peres, L.F., Rosa, A.S., Schroeder, W., Pereira, J.M.C., Giglio, L., Trigo, I.F., Setzer, A.W., 2019. How well do global burned area products represent fire patterns in the Brazilian Savannas biome? An accuracy assessment of the MCD64 collections. *Int. J. Appl. Earth Obs. Geoinf.* <https://doi.org/10.1016/j.jag.2019.02.010>.
- Rosário, N.E., Longo, K.M., Freitas, S.R., Yamasoe, M.A., Fonseca, R.M., 2013. Modeling the South American regional smoke plume: aerosol optical depth variability and surface shortwave flux perturbation. *Atmos. Chem. Phys.* 13, 2923–2938.
- Rozoff, C.M., Cotton, W.R., Adegoke, J.O., 2003. Simulation of St. Louis, Missouri, land use impacts on thunderstorms. *Journal of Applied Meteorology and Climatology*. [https://doi.org/10.1175/1520-0450\(2003\)042<0716:SOSLML>2.0.CO;2](https://doi.org/10.1175/1520-0450(2003)042<0716:SOSLML>2.0.CO;2).
- Saldiva, P.H.N., Lichtenfels, A.J.F.C., Paiva, P.S.O., Barone, I.A., Martins, M.A., Massad, E., Pereira, J.C.R., Xavier, V.P., Singer, J.M., Böhm, G.M., 1994. Association between air pollution and mortality due to respiratory diseases in children in São Paulo: a preliminary report. *Environ. Res.* <https://doi.org/10.1006/ENRS.1994.1033>.
- Sayer, A.M., Hsu, N.C., Bettenhausen, C., Lee, J., Kim, W.V., Smirnov, A., 2017. Satellite ocean aerosol retrieval (SOAR) algorithm extension to S-NPP VIIRS as part of the “deep blue” aerosol project. *J. Geophys. Res.: Atmosphere*. <https://doi.org/10.1002/2017JD027412>.
- Seinfeld, J.H., Pandis, S.N., 2016. *Atmospheric Chemistry and Physics: from Air Pollution to Climate Change*. John Wiley & Sons, Hoboken.
- Setzer, A., Pereira, M., 1991. Amazonia biomass burnings in 1987 and an estimate of their tropospheric emissions. *Ambio* 20, 19–22.
- Silva Dias, M.A.F., 2006. *Meteorologia, desmatamento e queimadas na Amazônia: Uma síntese de resultados do LBA*. *Rev. Bras. Meteorol.* 21, 190–199.
- Simpson, D., Benedictow, A., Berge, H., Bergström, R., Emberson, L.D., Fagerli, H., Flechard, C.R., Hayman, G.D., Gauss, M., Jonson, J.E., Jenkin, M.E., Nyíri, A., Richter, C., Semeena, V.S., Tsyro, S., Tuovinen, J.-P., Valdebenito, A., Wind, P., 2012. The EMEP MSC-W chemical transport model – technical description. *Atmos. Chem. Phys.* <https://doi.org/10.5194/acp-12-7825-2012>.
- Skamarock, W.C., Klemp, J.B., Dudhia, J., Gill, D.O., Barker, D., Duda, M.G., Powers, J.G., 2008. A Description of the Advanced Research WRF Version 3 (No. NCAR/TN-475+STR). University Corporation for Atmospheric Research. <https://doi.org/10.5065/D68S4MVH>.
- Song, S.-K., Shon, Z.-H., Kang, Y.-H., Kim, K.-H., Han, S.-B., Kang, M., Bang, J.-H., Oh, I., 2019. Source apportionment of VOCs and their impact on air quality and health in the megacity of Seoul. *Environ. Pollut.* <https://doi.org/10.1016/j.envpol.2019.01.102>.
- Souza, D.Z., Vasconcellos, P.C., Lee, H., Aurela, M., Saarnio, K., Teinila, K., Hillamo, R., 2014. Composition of PM_{2.5} and PM₁₀ collected at urban sites in Brazil. *Aerosol Air Qual. Res.* 14, 168e176. <https://doi.org/10.4209/aaqr.2013.03.0071>.
- Stein, O., Schultz, M.G., Bouarar, I., Clark, H., Huijnen, V., Gaudel, A., George, M., Clerbaux, C., 2014. On the wintertime low bias of Northern Hemisphere carbon monoxide found in global model simulations. *Atmos. Chem. Phys.* 14, 9295–9316. <https://doi.org/10.5194/acp-14-9295-2014>.
- Stockwell, W.R., Kirchner, F., Kuhn, M., Seefeld, S., 1997. A new mechanism for regional atmospheric chemistry modeling. *J. Geophys. Res.* <https://doi.org/10.1029/97JD00849>.
- Tewari, M., Chen, F., Wang, W., Dudhia, J., LeMone, M.A., Mitchell, K., Ek, M., Gayno, G., Wegiel, J., Cuenca, R.H., 2004. Implementation and Verification of the Unified NOAA Land Surface Model in the WRF Model. 20th Conference on Weather Analysis and Forecasting/16th Conference on Numerical Weather Prediction, pp. 11–15.
- Tie, X., Madronich, S., Li, G.H., Ying, Z.M., Zhang, R.Y., Garcia, A.R., Lee-Taylor, J., Liu, Y.B., 2007. Characterizations of chemical oxidants in Mexico City: a regional chemical dynamical model (WRF-Chem) study. *Atmos. Environ.* 41, 1989–2008.
- United Nations, Department of Economic and Social Affairs, Population Division, 2018. World urbanization prospects: the 2018 revision. <https://population.un.org/wup/Publications/>. (Accessed 13 July 2019).
- Vara-Vela, A., Andrade, M.F., Kumar, P., Ynoue, R.Y., Munoz, A.G., 2016. Impact of vehicular emissions on the formation of fine particles in the São Paulo metropolitan area: a numerical study with the WRF-Chem model. *Atmos. Chem. Phys.* <https://doi.org/10.5194/acp-16-777-2016>, 2016.
- Vara-Vela, A., Andrade, M.F., Zhang, Y., Kumar, P., Ynoue, R.Y., Souto-Oliveira, C.E., Lopes, F.J.S., Landulfo, E., 2018. Modeling of atmospheric aerosol properties in the

- São Paulo Metropolitan Area: impact of biomass burning. *J. Geophys. Res.* <https://doi.org/10.1029/2018JD028768>.
- Vasconcellos, P.C., Souza, D.Z., Sanchez-Cocoylo, O., Bustillos, J.O.V., Lee, H., Santos, F. C., Nascimento, K.H., Araújo, M.P., Saarnio, K., Teinila, K., Hillamo, R., €., 2010. Determination of anthropogenic and biogenic compounds on atmospheric aerosol collected in urban, biomass burning and forest areas in São Paulo, Brazil. *Sci. Total Environ.* 408 (23), 5836e5844. <https://doi.org/10.1016/j.scitotenv.2010.08.012>.
- Wang, Z.H., Bai, Y.H., Zhang, S.Y., 2005. A biogenic volatile organic compounds emission inventory for Yunnan Province. *J. Environ. Sci. (China)* 17 (3), 353–359, 2005.
- Wang, K., Zhang, Y., Yahya, K., Wu, S.-Y., Grell, G., 2015. Implementation and Initial Application of New Chemistry-Aerosol Options in WRF/Chem for Simulating Secondary Organic Aerosols and Aerosol Indirect Effects for Regional Air Quality. *Atmospheric Environment*. <https://doi.org/10.1016/j.atmosenv.2014.12.007>.
- Wang, N., Lyu, X.P., Deng, X.J., Guo, H., Deng, T., Li, Y., Yin, C.Q., Li, F., Wang, S.Q., 2016. Assessment of regional air quality resulting from emission control in the Pearl River Delta region, southern China. *Sci. Total Environ.* <https://doi.org/10.1016/j.scitotenv.2016.09.013>.
- Wechsler S. *Statistics at Square One*. ninth ed. London, UK: BMJ Publishing Group.
- Yu, M., Zhu, Y., Lin, C.-J., Wang, S., Xing, J., Jang, C., Huang, J., Huang, J., Jin, J., Yu, L., 2019. Effects of air pollution control measures on air quality improvement in Guangzhou, China. *J. Environ. Manag.* <https://doi.org/10.1016/j.jenvman.2019.05.046>.
- Zhang, Y., 2008. Online-coupled meteorology and chemistry models: history, current status, and outlook. *Atmos. Chem. Phys.* <https://doi.org/10.5194/acp-8-2895-2008>.
- Zhang, L., Lin, J., Qiu, R., Hu, X., Zhang, H., Chen, Q., Tan, H., Lin, D., Wang, J., 2018. Trend analysis and forecast of PM_{2.5} in Fuzhou, China using the ARIMA model. *Ecol. Indic.* <https://doi.org/10.1016/j.ecolind.2018.08.032>.